Response to reviewer #1

We thank the reviewer for her/his in depth review comments that have help us to improve the clarity of the manuscript. Kindly find below our responses to each of the comments (quoted between []). We hope that our responses will address the main issues and that the changes made will convince that the IASI HNO_3 dataset has the potential to contribute to stratospheric studies and, more particularly, to the time evolution of the polar processes.

Major comments

[The major part of the data (2008-2016) reported in this manuscript was already published in Ronsmans et al. (2018), also together with temperatures at 50 hPa. For example, Fig. 4 (top) of the actual manuscript is a zoom of Fig. 3 of Ronsmans et al. (2018) to the southern latitudes with one Antarctic winter added.]
This paper indeed builds on the study of Ronsmans et al. (2018) but it goes a step further in showing the potential of the IASI-HNO_3 dataset for polar stratospheric studies, which was not detailed in Ronsmans et al. (2018). If MLS allows resolving the HNO_3 profile between 11 km and 30 km, the potential of IASI lies in its exceptional spatial and temporal sampling. We demonstrate here that despite its limited vertical sensitivity forcing us to consider one total column, the information content that lies in the low-middle stratosphere is good enough to expand on polar stratospheric denitrification studies, usually performed using limb sounder measurements, and to continue their long-term record given the end of limb-observations in the microwave and thermal infrared spectral region.

[While Ronsmans et al. (2016) provide a first validation of the observations by comparison with FTIR solar absorption measurements, a characterization given the extreme conditions within the dark Antarctic polar vortex is missing. This is one of the majors concerns why I think the paper should not be published in ACP in its present form. However, it should be quite straightforward to provide at least a first comparison with HNO3 observations by the Microwave Limb Sounder (MLS) which has a large temporal and spatial overlap with the IASI dataset.]
The referee is kindly invited to refer to the figure 3 (top and bottom panels) of Ronsmans et al. (2016) that presents the global distributions of the degrees of freedom for signal (DOFS, top panels) and of the altitude of maximum sensitivity of IASI to the HNO_3 profile, separately for January (left) and July (right) 2011, when the strong HNO_3 depletion occurs within the cold Antarctic winter. Figure 3 of Ronsmans et al. (2016) clearly shows DOFS of around 0.95-1.05 inside the Antarctic polar vortex, demonstrating the ability of IASI to measure a total column of HNO_3 even above these coldest regions. It is also worth to note here that the measurements characterized by a low vertical resolution (DOFS < 0.9) or a poor spectral fit have been filtered out of this analysis. This is now better mentioned in Section 2 of the revised manuscript:

"Quality flags similar to those developed for O_3 in previous IASI studies (Wespes et al., 2017) were applied a posteriori to exclude data (i) with a corresponding poor spectral fit (e.g. based on quality flags rejecting biased or sloped residuals, fits with maximum number of iteration exceeded), (ii) with less reliability (e.g. based on quality flags rejecting suspect averaging kernels, data with less sensitivity characterized by a DOFS lower than 0.9) or (iii) with tropospheric cloud contamination (defined by a fractional cloud cover larger than 25 %)."

Despite the fact that a validation of the IASI measurements within the Antarctic polar vortex against ground-based FTIR measurements could not be provided (these observations requiring sunlight), we agree that an evaluation of the IASI measurements in the Antarctic night was missing. Hence, as suggested by the referee, we have preformed cross-comparison with observations by MLS in three equivalent latitude bands (see Figure 1 here below). We would like to point out that we here compare total columns measured by IASI with VMR measured by MLS at several pressure levels that cover the highest sensitivity of IASI (at ~50 hPa, ~70 hPa and ~30 hPa for the sake of the comparison). Hence, the comparison of IASI columns with MLS measurements is mostly qualitative at this stage and differences are expected for this reason. Note also that we have preferred comparing IASI HNO_3 columns with VMR measured by MLS at specific levels instead of integrated columns calculated from MLS, given the difference in the sensitivity profile between IASI and MLS, the non-negligible IASI sensitivity to HNO_3 in the troposphere where MLS does not measure HNO_3 etc, which makes the integrated columns from IASI vs MLS not directly comparable. It should be pointed out finally that part of the differences between IASI and MLS are likely due to the different number of co-located data within the 2.5°x2.5° grid cells considered here for the comparison, with a much larger number of observations for IASI (through the quality filtering) than for MLS.

Despite this, the comparison shows similar spatial and seasonal variations between IASI total HNO_3 columns and MLS VMR between ~70 and 30 hPa in the different latitude bands, in particular, in the southernmost equivalent latitudes (see top panel). The strong HNO_3 depletion is well captured by both IASI and MLS measurements with a perfect match for the onset of the depletion. It further supports the good sensitivity of IASI to HNO_3 in the range of these pressure levels, justifying the methodology used in this study.

The cross-comparison with MLS is indeed insightful and gives further credit on the IASI observations during the polar night. That comparison figure between IASI and MLS has therefore been included in Section 2 of the revised manuscript and the text was changed to:
"In order to expand on the comparisons against FTIR measurements which is impossible during the polar night, Figure 1 (top panel) presents the time series of daily IASI total HNO_3 columns co-located with MLS VMR measurements within 2.5x2.5 grid boxes at three pressure levels (at 30, 50 and 70 hPa), averaged in the 70°S–90°S equivalent latitude band. Similar variations in HNO_3 are captured by the two instruments with an excellent agreement for the timing of the strong HNO_3 depletion within the inner vortex core. IASI HNO_3 variations generally match well those of MLS HNO_3 in each latitude band (see Figure 1 bottom panel for the 50°S–70°S equivalent latitude band; the other bands are not shown here)."

Specific comments

[L3, 'good vertical sensitivity': This has not been shown in this paper. It is necessary to demonstrate this for the dataset discussed here given the cold Antarctic stratosphere.]
As stated in the text, we here refer to "a good vertical sensitivity in the low and middle stratosphere", not to a good vertical resolution of the measurement.

As mentioned in the manuscript, this paper builds on the previous studies of Ronsmans et al. (2016) and (2018). Despite a poor vertical resolution between the retrieved layers forcing us to consider a total column, the sensitivity of IASI to HNO_3 was shown to vary with altitude and to be highest in the low-middle stratosphere, even within the cold Antarctic polar vortex (Ronsmans et al. (2016)). This means that the variability in the measured total column is mainly representative of that layer. As said above, we recall here that similarly to the earlier studies, HNO_3 measurements characterized by a poor spectral fit or by a low vertical sensitivity (DOFS < 0.9) have been filtered out of this analysis. This is now clearly mentioned in Section 2 of the revised manuscript:

"Quality flags similar to those developed for O_3 in previous IASI studies (Wespes et al., 2017) were applied a posteriori to exclude data (i) with a corresponding poor spectral fit (e.g. based on quality flags rejecting biased or sloped residuals, fits with maximum number of iteration exceeded), (ii) with less reliability (e.g. based on quality flags rejecting suspect averaging kernels, data with less sensitivity characterized by a DOFS lower than 0.9) or (iii) with tropospheric cloud contamination (defined by a fractional cloud cover larger than 25 %)."

[L8, 'denitrification': Are you certain, that 'denitrification' is also used for the uptake of HNO3 in particles? Perhaps 'removal from the gas phase'.]
We thank the referee for this remark. We are of course aware that the so-called "denitrification" defines the permanent removal of NOy from an airmass due to the gravitational sedimentation of NOy-containing particles. We agree that, from IASI, we can only measure a "removal from the gas phase", caused by sequestration into particles with or without sedimentation. Careful attention has now been made in the manuscript to avoid abusive use of the term "denitrification". Hence, "onset of HNO_3 denitrification" has been changed to "the onset of HNO_3 depletion" where appropriated in the revised manuscript. The title has also been changed accordingly to:
"Polar stratospheric HNO_3 depletion surveyed from a decadal dataset of IASI total columns".

[L59, 'a maximum sensitivity in the mid-stratosphere around 50 hPa': This must be shown here for the extreme conditions in the Antarctic vortex - also since all later analyses in the paper use temperatures at 50 hPa. What is the vertical variability of this level of maximum sensitivity within the development inside the vortex, especially later in the winter when, due to sedimentation of PSC particles, HNO3 concentrations at those levels are very low?]
See our responses to the general comments. Here again, we refer to the figure 3 (top and bottom panels) of Ronsmans et al. (2016) that presents the global distributions of the degrees of freedom for signal (DOFS, top panels) and of the altitude of maximum sensitivity of IASI to the HNO_3 profile (bottom panel), separately for January (left) and July (right) 2011, when the strong HNO_3 depletion occurs within the cold Antarctic winter. It shows clearly that the altitude of maximum sensitivity of the total columns is invariant at equatorial and tropical latitudes, whereas it varies with seasons at middle and polar latitudes. Above the Antarctic, the altitude of maximum sensitivity varies between ~9 km in summer and ~22 km in winter. The variations of the altitude of maximum sensitivity follow the altitude variations of maximum HNO_3 concentrations.

This is now more explicit at several places in the revised manuscript; e.g. in Section 1: "IASI provides reliable total column measurements of HNO_3 characterized by a maximum sensitivity in the low-middle stratosphere around 50 hPa (20 km) during the dark Antarctic winter (Ronsmans et al., 2016; 2018) …" and in Section 2: "… the largest sensitivity of IASI in the region of interest, i.e. in the low and mid-stratosphere (from 70 to 30 hPa), where the HNO_3 abundance is the highest (Ronsmans et al., 2016).

In order to convince the referee that IASI measurements capture the expected variations of HNO_3 within the polar night, we provide in Figure 2 below examples of vertical HNO_3 profiles retrieved within the dark Antarctic vortex (above Arrival Height) and outside the vortex (above Lauder). The retrieved profiles are shown along with their associated total retrieval error and averaging kernels (the total column AvK and the so-called "sensitivity profile" are also represented). The sum of the averaging kernels indicates how the true state at a specific altitude changes the retrieved total column, i.e. the altitude to which the retrieved total column is mainly sensitive/representative. Above Arrival Height during the dark Antarctic winter, we clearly see depleted HNO_3 levels in the low and mid-stratosphere and the altitude of maximum sensitivity at around 30 hPa. At Lauder on the contrary, HNO_3 levels larger than the a priori are observed in the stratosphere with a larger range of maximum sensitivity.

[L79, ‘The total columns yield a total retrieval error of 10% and a low bias (10.5%) compared to ground-based FTIR measurements (Hurtmans et al., 2012; Ronsmans et al., 2016).’: As these numbers are used also later in the manuscript, their validity has to be confirmed for the condition in the dark vortex, which cannot be achieved with comparisons to sun-dependent FTIR observations. As mentioned above, I strongly suggest to perform comparisons with the MLS dataset.]
Figure 4 of Ronsmans et al. (2016) illustrates the global distribution of the total retrieval error for HNO_3 (integrated over 5 to 35 km) separately for January (left) and July (right) over the period of the IASI measurements. The mid- and polar latitudes are characterized by low total retrieval errors of around ~3-5% - which corresponds to a reduction by a factor of 18-30 compared to the prior uncertainty (90%) and indicates a real gain of information – except above Antarctica during wintertime where the errors reach 25%. They are explained by (1) a weaker sensitivity (i.e. a larger smoothing error which represents in all cases the larger source of the retrieval error) above such cold surface (DOFS of ~0.95 within the dark Antarctic vortex – see figure 3 of Ronsmans et al., 2016) and by (2) a misrepresentation of the wavenumber-dependent surface emissivity above ice surface (Hurtmans et al., 2012). This is made more explicit in Section 2 of the revised manuscript:

“The total columns are associated with a total retrieval error ranging from around 3% at mid- and polar latitudes to 25% above cold Antarctic surface during winter (due to a weaker sensitivity above very cold surface with a DOFS of ~0.95 and to a poor knowledge of the seasonally and wavenumber-dependent emissivity above ice surfaces which induces larger forward model errors), and a low bias (lower than 12%) in polar regions over the altitude range where the IASI sensitivity is largest, when compared to ground-based FTIR measurements (see Hurtmans et al., 2012; Ronsmans et al., 2016 for more details).”

A validation against ground-based sun-dependent FTIR measurements could not be provided during the dark Antarctic winter, we refer on the good agreement with MLS (suggested by the referee) to underline the potentiality of IASI to detect the HNO_3 variations as well within the Antarctic winter (see general comment).

[L105, ‘These high HNO_3 levels result from low sunlight…’: This is not the only, and probably not the central explanation for the increasing column amounts. Dynamical effects on total columns of stratospheric gases (downwelling within the vortex) have to be considered.]
We thank the referee for this correction. The sentence has been rewritten as follows:

“These high HNO_3 levels result from low sunlight, preventing photodissociation, along with the heterogeneous hydrolysis of N_2O_5 to HNO_3 during autumn before the formation of polar stratospheric clouds (Keys et al., 1993; Santee et al., 1999; Urban et al., 2009; DeZafra et al., 2001). This period also corresponds to the onset of the deployment of the southern polar vortex which is characterized by strong diabatic descent with weak latitudinal mixing across its boundary, isolating polar HNO_3-rich air from lower latitudinal airmasses.”

[Figure 2: I think the vertical dashed line ‘10Jun09’ does not fit to the minimum of the solid blue curve (?)]
The referee is right; there was a bug for the automatically detection of the drop temperature, as well as for the detection of the corresponding dates in this figure. The figure has been corrected. The position of the drop temperatures does now perfectly match the yearly minima of the total HNO_3 second derivative. An average drop temperature over the ten years of IASI of 194.2 +/- 3.8 K is now calculated, which is even closer to T_{NAT}.

[L154, 'in the areas of potential vorticity smaller than -10 …': PV at which potential temperature level is used here?]

As mentioned in Section 2 of the submitted manuscript, "the potential vorticity (PV) fields are taken from the ECMWF ERA Interim Reanalysis dataset at the potential temperature of 530 K (corresponding to ~20 km altitude where the IASI sensitivity to HNO_3 is the highest during the Southern Hemisphere (S.H.) winter (Ronsmans et al., 2016)".

[L159, 'Note that the HNO_3 time series has been smoothed': As the drop temperatures (and dates) are introduced as the central new method presented in the manuscript, it is necessary to explore their behaviour in more detail. Can you give an estimate of the error of this measure by considering e.g. the effect of the numerical smoothing. Please show also the 1st derivative to be able to judge on the uncertainties of the 2nd derivative. How do the drop temperatures vary when using different pressure levels (e.g. 70 hPa)?]

As explained in the text, we actually only used a simple robust spline smoothing function to fill gaps in the time series, hence it has no particular impact on the detection of the drop temperature and its corresponding date.

Figure 3 here below represents the figure 2 of the manuscript along with the 1st derivative of HNO_3 total column with respect to time superimposed, as asked by the referee. We can clearly see that the minima of the 2nd derivative match or just precede those of the 1st derivative of total HNO_3 with respect to time.

Figure 4 below represents the figure 2 of the manuscript but for the temperature at 30 hPa (top panel) and 70 hPa (bottom panel) for the sake of comparison. As expected, the drop temperatures are the lowest when using the temperatures at 30 hPa. They vary from 185-195 K (~192K on average) at 30 hPa to 195-204 K (~198 K on average) at 70 hPa with values of ~189-202 K (~194 K on average) at 50 hPa.

As explained in the manuscript, the use of the 195 K at 50 hPa as single level for the analysis is justified by the fact that it corresponds best to the maximum of IASI vertical sensitivity during the polar night (see Figure 3 of Ronsmans et al. 2016 and responses to related comments above); another justification is found a posteriori by the consistency between the 195 K threshold temperature taken at 50 hPa and the onset of the strong total HNO_3 depletion seen by IASI, which matches the NAT development that occurs in June around that level. However, we fully agree that the HNO_3 abundances over a large part of the stratosphere (between 70 and 30 hPa) contribute to the total HNO_3 variations detected by IASI and that this inevitably affects the drop temperature calculation at 50 hPa. In order to address this issue, we have added in the manuscript the range of drop temperatures when calculated at these two other pressure levels (from 185 K to 204 K); this indeed allows the reader to better judge on the uncertainty of the drop temperature at 50 hPa (189-202 K). We thank the referee for his suggestion. The text in the revised manuscript is changed to:

"… Nevertheless, given the range of maximum IASI sensitivity to HNO_3 around 50 hPa, typically between 70 and 30 hPa (Ronsmans et al., 2016), the drop temperatures are also calculated at these two other pressure levels (not shown here) to estimate the uncertainty of the calculated drop temperature defined in this study at 50 hPa. The 30 hPa and 70 hPa drop temperatures range respectively over 185.7 K – 194.9 K and over 194.8 K – 203.7 K, with an average of 192.0 +/- 2.9 K and 198.0 +/- 3.2 K (1σ standard deviation) over the ten years of IASI. The average values at 30 hPa and 70 hPa fall within the 1σ standard deviation associated with the average drop temperature at 50 hPa. It is also worth noting the agreement between the drop temperatures and the NAT formation threshold at these two pressure levels (T_{NAT} ~193 K at 30 hPa and ~197 K at 70 hPa) (Lambert et al., 2016)."

[L184, 'The calculated drop temperatures vary significantly between 180 and 210 K. These high extremes are only found in very few cases and should be considered with caution as they correspond to specific regions above ice shelves with emissivity features that are known to yield errors in the IASI retrievals': I find the discussion around the deviations of the drop temperatures very confusing. At the beginning of the manuscript it is stated, that the error of the measured total column amounts is in the order of 10%. Here it is argued that 'above ice shelves' it might be higher. Also, in Fig. 5 one can see that there are large regions over eastern Antarctica where drop temperatures are often clearly above 195K even inside the red circles. This is not explained satisfactorily in the manuscript. Here, again, it would be important to investigate on the reliability, consistency and homogeneity of the IASI HNO3 values. As mentioned above, this could be accomplished with a comparison to MLS observations.]
See our response above about the characterization of the HNO_3 retrievals in terms of total retrieval error and of its spatial/temporal distribution: The largest errors (25%) are found above Antarctica during wintertime and are due to (1) a weaker sensitivity (i.e. a larger smoothing error which represents in all cases the larger source of the retrieval error) above such cold land surface (DOFS of ~0.95 within the dark Antarctic vortex – see figure 3 of Ronsmans et al., 2016) and to (2) a poor knowledge of the (seasonally and wavenumber-dependent) emissivity of ice surfaces (Hurtmans et al., 2012). This is now clearly mentioned in Section 2 of the revised manuscript.

Bright land surface such as desert or ice might in some cases lead to poor HNO_3 retrievals due to a poor knowledge of the wavenumber-dependent emissivity above such surfaces, which can alter the retrieval by compensation effects (Wespes et al., 2009). FORLI relies on the monthly climatology of surface emissivity built by Zhou et al. (2011) from several years of IASI measurements on a 0.5x0.5 grid and for each 8461 IASI spectral channels when available, or on the MODIS climatology that is unfortunately restricted to only 12 channels in the IASI spectral range; see Hurtmans et al. (2012) for more details. Although wavenumber-dependent surface emissivity atlases are used in FORLI, it is clear that this parameter remains critical and causes poorer retrievals that, in some instances, pass the posterior filtering. The total HNO_3 columns over eastern Antarctica which show drop temperatures much above 195K might precisely be related to this. We have made this clear in Section 4.2 of the revised version:

"…emissivity features that are known to yield errors in the IASI retrievals (Hurtmans et al., 2012; Ronsmans et al., 2016). Indeed, bright land surface such as ice might in some cases lead to poor HNO_3 retrievals. Although wavenumber-dependent surface emissivity atlases are used in FORLI (Hurtmans et al., 2012), this parameter remains critical and causes poorer retrievals that, in some instances, pass through the series of quality filters and affect the drop temperature calculation."

[L195, 'Overall, despite these limitations, the spatial variability in the drop 50 hPa temperatures for IASI total HNO_3 is well in agreement with the natural variation in PSCs nucleation temperatures': Given the extended areas where the drop temperatures are larger than 195K, this statement is not convincing.]
The sentence has been rewritten for clarity:

"Except above some parts of Antarctica which are prone to larger errors, the overall range in the drop 50 hPa temperature for total HNO_3, inside the isocontour for the averaged temperature of 195 K, typically extends from ~187 K to 195 K, which fall within the range of PSCs nucleation temperature at 50 hPa …".

Furthermore, in response to G. Manney and M. Santee, the contour of $-10\times10^{-5}K.m^2.kg^{-1}.s^{-1}$ based on the minimum PV encountered at 50 hPa over the 10 May to 15 July period as well as the isocontours of 195 K at 50 hPa for the averaged temperatures and the minima over the same period are also now represented in the revised Fig.5 and the distribution of the drop temperatures is much better described and explained in the revised version:

"The averaged isocontour of 195 K encircles well the area of HNO_3 drop temperatures lower than 195 K, which means that the bins inside that area characterize airmasses that experience the NAT threshold temperature during a long time over the 10 May – 15 July period. That area encompasses the inner vortex core (delimited by the isocontour of -10×10^{-5}K.m^2.kg^{-1}.s^{-1} for the averaged PV) and show pronounced minima (lower than -0.5 x10^{14} molec.cm^{-2}.d^{-2}) in the second derivative of the HNO_3 total column with respect to time (not shown here), which indicate a strong and rapid HNO_3 depletion.
The area enclosed between the two isocontours of 195 K for the temperatures, the averaged one and the one for the minimum temperatures, show higher drop temperatures and weakest minima (larger than -0.5 x10^{14} molec.cm^{-2}.d^{-2}) in the second derivative of the HNO_3 total column (not shown). That area is also enclosed by the isocontour of -10×10^{-5}K.m^2.kg^{-1}.s^{-1} for the minimum PV, meaning that the bins inside correspond, at least for one day over the 10 May – 15 July period, to airmasses located at the inner edge of the vortex and characterized by temperature lower than the NAT threshold temperature. The weakest minima in the second derivative of total HNO_3 (not shown) observed in that area indicate a weak and slow HNO_3 depletion and might be explained by a short period of the NAT threshold temperature experienced at the inner edge of the vortex. It could also reflect a mixing with strong HNO_3-depleted and colder airmasses from the inner vortex core. The mixing with these "already" depleted airmasses could also explained the higher drop temperatures detected in those bins. Finally, note also that these high drop temperatures are generally detected later (after the HNO_3 depletion occurs, i.e. after the 10 May – 15 July period considered here – not shown), which supports the transport, in those bins, of earlier HNO_3-depleted airmasses and the likely mixing at the edge of the vortex."

[L204, 'denitrification phase': See statement about 'denitrification' above.]
See our response above.

[L230, 'To the best of our knowledge, it is the first time that such a large satellite observational data set of stratospheric HNO3 concentrations is exploited to monitor the evolution HNO3 versus temperatures.': This sounds somehow exaggerated given all the previous work on HNO3/temperature/PSCs, e.g. by use of the MLS dataset and also since the correlation with temperature has already been shown in Ronsmans et al., 2018.]
We here simply refer to the unprecedented potential of IASI in terms of its exceptional spatial and temporal sampling. Ronsmans et al. (2018) also referred to the IASI dataset and correlations with temperature were done but in a lesser extent. In order to avoid overselling, the sentence has been rewritten:
"We show in this study that the IASI dataset allows capturing the variability of stratospheric HNO_3 throughout the year (including the polar night) in the Antarctic. In that respect, it offers a new observational means to monitor the relation of HNO_3 to temperature and the related formation of PSCs."

Technical comments:

L27, '(e.g. (Toon…))': I think the inner bracket level is not necessary.
L30, 'sedimentation(Lambert …): Space missing
L34, 'temperature': 'temperatures'
L51: Bracket levels?
L102, 'The red vertical line in Fig. 1a and Fig. 1b': There is no vertical red line in Fig. 1a. You mean horizontal?
L106, references: Brackets seem wrong.

Figure 2, caption, ‘in the70—’: Space missing.
L155, ‘and the total HNO3 depletion are the coldest’: Makes no sense.
L164, ‘temperature are’: ‘temperatures are’

All the technical comments have been corrected.

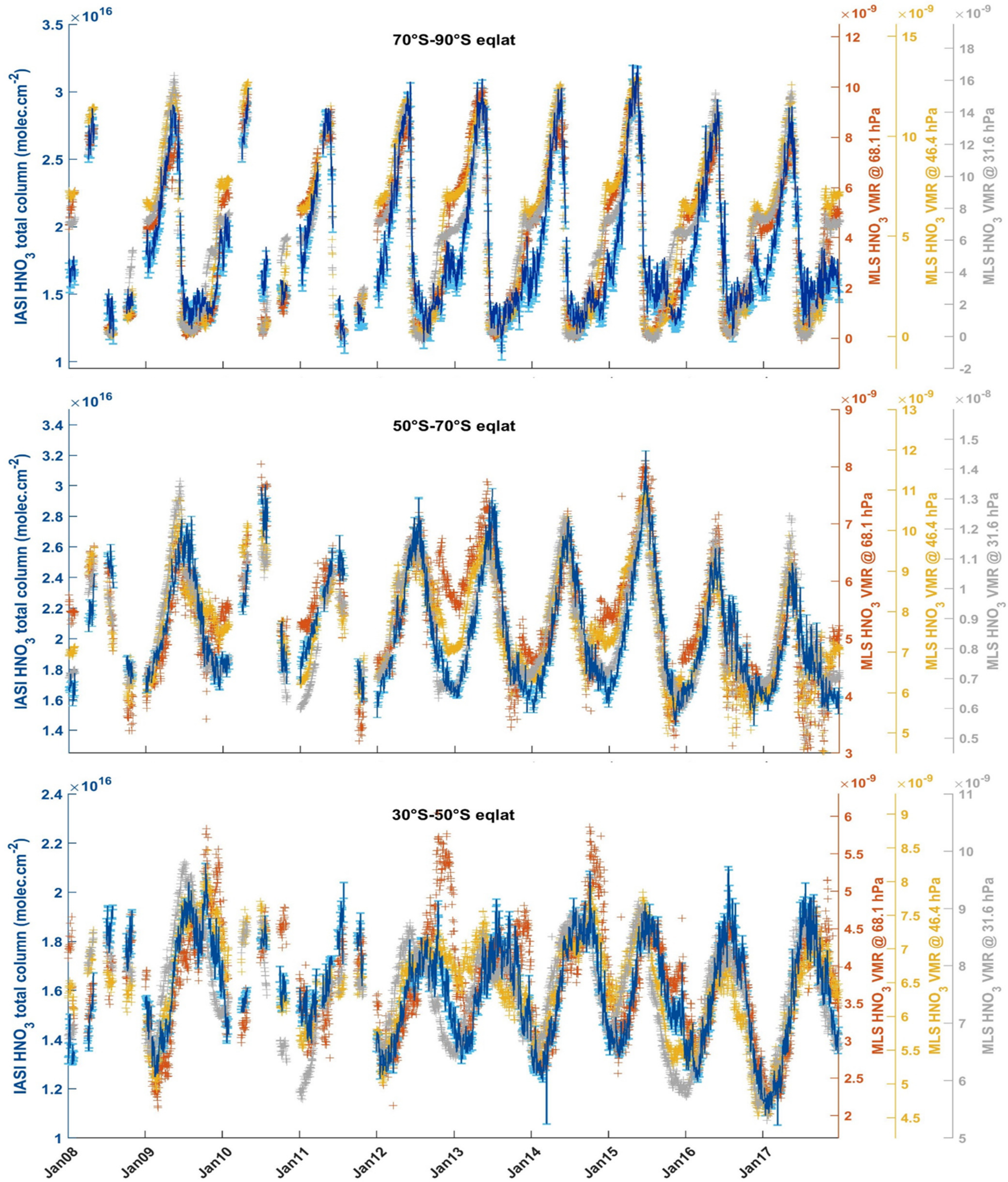

Figure 1. Time series of daily IASI total HNO_3 column (blue, left y-axis) co-located with MLS and of MLS VMR HNO_3 within 2.5x2.5 grid boxes at three pressure levels (at 30, 50 and 70 hPa; right y-axis), averaged in the 70°S–90°S (top panel), the 50°S–70°S (middle panel) and in the 30°S–50°S (bottom panel) equivalent latitude bands. The error bars (light blue) represents 3σ, where σ is the standard deviation around the IASI HNO_3 daily average.

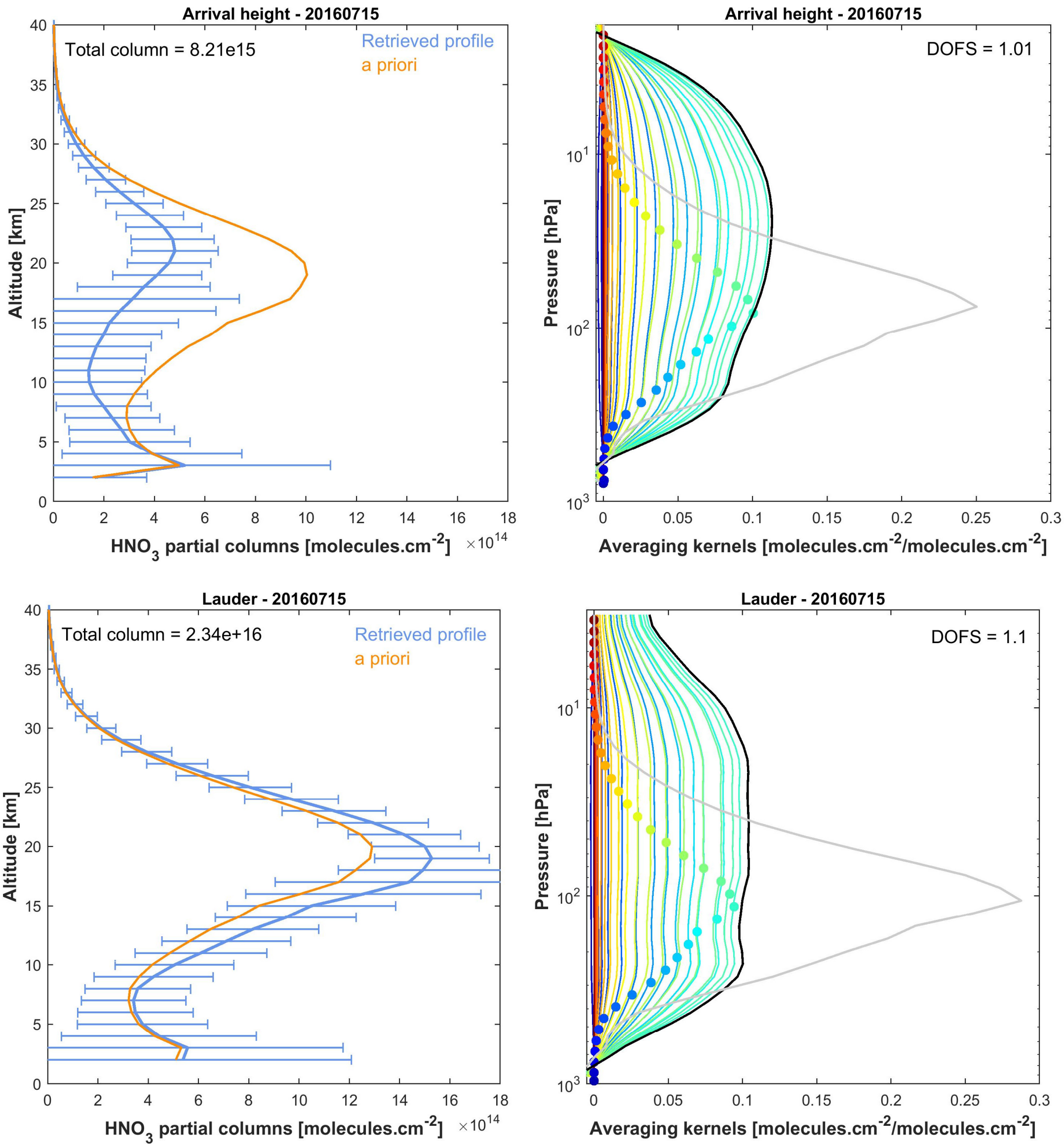

Figure 2. Examples of IASI HNO_3 vertical profiles (in molec.cm^{-2}) with corresponding averaging kernels (in molec.cm-^{2}/molec.cm-^{2}; with the total column averaging kernels (black) and the sensitivity profiles (grey)) above Arrival Height (77.49°S, 166.39°E, top panels) and Lauder (45.03°S, 169,40°E; bottom panels). The error bars associated with the HNO_3 vertical profile represent the total retrieval error. The a priori profile is also represented. The total column and the DOFS values are indicated.

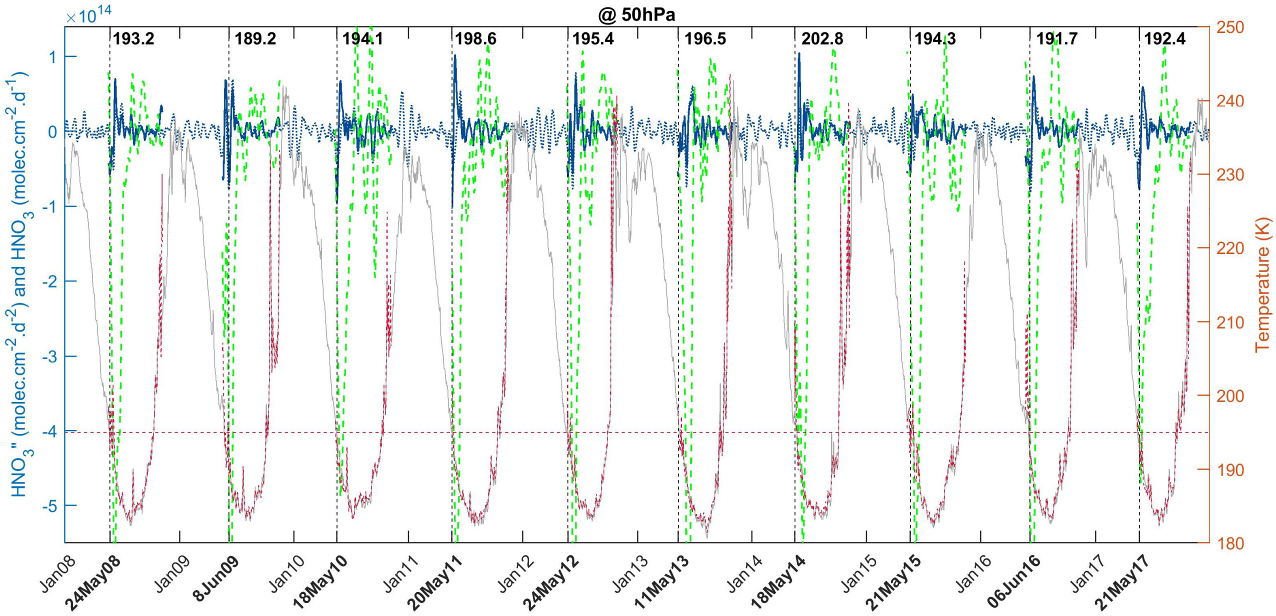

Figure 3. Time series of total HNO_3 first derivative (green, left y-axis), of total HNO_3 second derivative (blue, left y-axis) and of the temperature at 50 hPa (red, right y-axis), in the region of potential vorticity lower than -10 x10^{-5} $K.m^2.kg^{-1}.s^{-1}$. The red horizontal line corresponds to the 195 K temperature. The vertical dashed lines indicate the second derivative minimum in HNO_3 for each year. The corresponding dates (in bold, on the x-axis) and temperatures are also indicated. The time series of total HNO_3 second derivative (dashed blue) and of temperature at 50 hPa (grey) in the70–90°S Eqlat band are also represented.

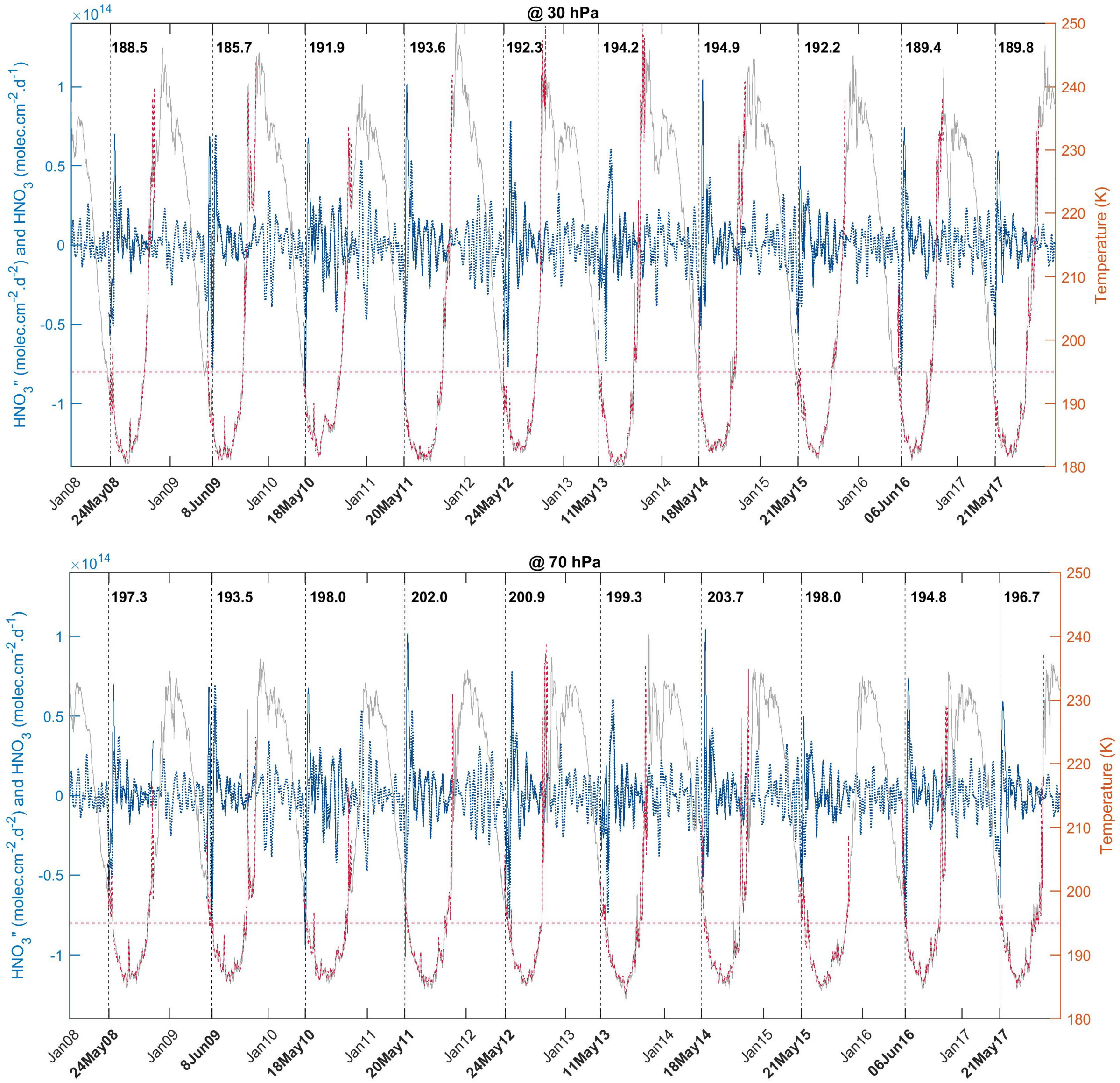

Figure 4. Same as Figure 3 but for the temperature at 30 hPa (top panel) and 70 hPa (bottom panel).

Response to reviewer #3

We thank the reviewer for her/his in depth review comments that have help us to improve the clarity of the manuscript. Kindly find below our responses to each of the comments (quoted between []). We hope that our responses will address the main issues and that the changes made will convince that the IASI HNO_3 dataset has the potential to contribute to stratospheric studies and, more particularly, to the time evolution of the polar processes.

Major comments

[The description of the polar HNO3 variation presented in the paper is already well known from numerous other studies.]

The purpose of this paper is to demonstrate the interest of IASI for HNO_3 stratospheric studies (Ronsmans et al., 2018) after having undergone a rigorous validation exercise (Ronsmans et al., 2016). If limb measurements allows resolving the HNO_3 profile in the stratosphere, the potential of IASI lies in its exceptional spatial and temporal sampling. We demonstrate here that despite its limited vertical resolution forcing us to consider one total column, the information content that actually lies in the low and middle stratosphere offers potential to expand on previous polar stratospheric denitrification studies, usually performed using limb sounder measurements, and to continue the long-term records of HNO_3 started with the latter. We have tried in this paper not to repeat too much of our earlier work but some duplication was unavoidable; in particular, with respect to vertical sensitivity and errors (these are two aspects that referee1 finds in fact insufficiently described here).

[The lack of vertical resolution in the IASI HNO3 measurements severely limits the interpretation of the results and precludes differentiation between denitrification and renitrification e.g. consider the effect of the vertical integration through depleted higher layers overlaying lower enhanced layers.]

We understand that the referee sees this as a limitation. However, despite the lack of <u>vertical resolution</u>, which is recognized in the paper and which forces us to consider total HNO_3 columns, IASI is characterized by a good <u>sensitivity</u> to HNO_3 <u>at specific levels</u>, in particular, in the range between ~70 hPa to ~30 hPa in the southernmost latitude in winter and as such it provides an adequate means to investigate the stratospheric processes in the polar nights.

In order to justify this further, we would like to refer to the figure 3 (top and bottom panels) of Ronsmans et al. (2016) that presents global distributions of the degrees of freedom for signal (DOFS, top panels) and of the altitude of maximum sensitivity of IASI to the HNO_3 profile (bottom panel), separately for January (left) and July (right) 2011, when the strong HNO_3 depletion occurs within the cold Antarctic winter. It shows clearly that the altitude of maximum sensitivity of the total columns is invariant at equatorial and tropical latitudes, whereas it varies with seasons at middle and polar latitudes. Above the Antarctic, the altitude of maximum sensitivity varies between ~9 km in summer and ~22 km in winter. The variations of the altitude of maximum sensitivity follow the altitude variations of maximum HNO_3 concentrations.

We agree that the IASI sensitivity was insufficiently put forward in the text. We made it more explicit at several places in the revised manuscript; e.g. in Section 1: "IASI provides reliable total column measurements of HNO_3 characterized by a maximum sensitivity in the low-middle stratosphere around 50 hPa (20 km) during the dark Antarctic winter (Ronsmans et al., 2016; 2018) …" and in Section 2: "… the largest sensitivity of IASI in the region of interest, i.e. in the low and mid-stratosphere (from 70 to 30 hPa), where the HNO_3 abundance is the highest (Ronsmans et al., 2016)."

[Although the IASI HNO3 data has much better 2D horizontal resolution than any other measurement this has not been developed as a tool to provide information beyond that of satellite instruments that measure only along the orbit track.]
We do not fully agree. The determination of the drop temperature using the second derivative exploits the large dataset of daily IASI measurements. Furthermore, the spatial distributions of the drop temperature calculated at 50hPa, which are presented in the figure 5 of the manuscript, do actually take advantage of the excellent spatial/temporal resolution of IASI to provide information throughout the entire vortex and outside. This would probably not be feasible with other types of measurements.

[CALIOP PSC information is available for the same time frame, why was this not used? Certainly, PSC volumes vs time would be helpful in providing the underlying interannual variability of PSC types (NAT, STS, ice) to compare with the resulting drop temperatures derived from IASI. Similarly, at least some comparisons of the IASI HNO3 column with integrated column calculated from Aura MLS are necesssary to establish the validity of the measurements in the most severly depleted inner vortex core.]
Thank you for this comment. It is certainly a good idea to use the CALIOP measurements in support but this goes beyond the goal of this paper, which is to demonstrate the capability of IASI to measure HNO_3 columns that are relevant for stratospheric studies. Using CALIOP PSC information and, in particular, comparing the spatial distributions of IASI derived drop temperatures (Figure 5 of the revised paper) with maps of CALIOP PSC would be very interesting in order to go a step further in the analyses of the underlying HNO_3 condensation processes, but it will be challenging and add significant complexity given the high variability in the distribution of PSC types.

Regarding the second point on a comparison with MLS, we fully agree that this is highly relevant; it was also a request of referee#1. We provide here below a comparison with observations by MLS in three equivalent latitude bands (see Figure 1). We would like to point out that we here compare total columns measured by IASI with VMR measured by MLS at several pressure levels that cover the highest sensitivity of IASI (at ~50 hPa, ~70 hPa and ~30 hPa for the sake of the comparison). Hence, the comparison of IASI columns with MLS measurements is mostly qualitative at this stage and differences are expected for this reason. Note also that we have preferred comparing IASI HNO_3 columns with VMR measured by MLS at specific levels instead of integrated columns calculated from MLS, given the difference in the sensitivity profile between IASI and MLS, the non-negligible IASI sensitivity to HNO_3 in the troposphere where MLS does not measure HNO_3 etc, which makes the integrated columns from IASI vs MLS not directly comparable. It should be pointed out finally that part of the differences between IASI and MLS are likely due to the different number of co-located data within the 2.5°x2.5° grid cells considered here for the comparison, with a much larger number of observations for IASI (through the quality filtering) than for MLS.

Despite this, the comparison shows similar spatial and seasonal variations between IASI total HNO_3 columns and MLS VMR between ~70 and 30 hPa in the different latitude bands, in particular, in the southernmost equivalent latitudes (see top panel). The strong HNO_3 depletion is well captured by both IASI and MLS measurements with a perfect match for the onset of the depletion. It further supports the good sensitivity of IASI to HNO_3 in the range of these pressure levels, justifying the methodology used in this study.

The cross-comparison with MLS is indeed insightful and gives further credit on the IASI observations during the polar night. That comparison figure between IASI and MLS has therefore been included in Section 2 of the revised manuscript and the text was changed to:

"In order to expand on the comparisons against FTIR measurements which is impossible during the polar night, Figure 1 (top panel) presents the time series of daily IASI total HNO_3 columns co-located with MLS VMR measurements within 2.5x2.5 grid boxes at three pressure levels (at 30, 50 and 70 hPa), averaged in the 70°S–90°S equivalent latitude band. Similar variations in HNO_3 are captured by the two instruments with an excellent agreement for the timing of the strong HNO_3 depletion within the inner vortex core. IASI HNO_3 variations generally match well those of MLS HNO_3 in each latitude band (see Figure 1 bottom panel for the 50°S–70°S equivalent latitude band; the other bands are not shown here)."

[Regarding the sensitivity of the IASI column HNO3 measurements, I suggest presenting a few examples of vertical HNO3 profiles (from a model or data), ranging from non-depleted to extreme depletion with calculations of the corresponding calculated integrated IASI column. This would help to indicate the sensitivity of the column measurement to changes in the vertical distribution of HNO3 ... i.e. generate profiles of the change in the IASI column HNO3 wrt the actual change in HNO3 at a level, j, d(column)/d(HNO3)j.]

This is an example of information reported in earlier work and that we have tried not to repeat extensively here. To summarize, the validation study of Ronsmans et al. (2016) provides a complete characterization of the IASI HNO_3 retrievals: it shows example of vertical HNO_3 profiles along with the total retrieval error, the a apriori profiles and associated averaging kernels profiles ($d(HNO3_{ret})i/d(HNO3_{true})j$), along with the total column averaging kernel ($d(column_{ret})/d(HNO3_{true})j$) and the sensitivity profile ($d(HNO3_{ret})i/d(column_{true})$), were already given in Figures 1 and 2 of that study. Note that the averaging kernel profile describes how the true state changes the estimate at a specific altitude, i.e. how the retrieval smooths the true profile. The sum of the elements of an averaging kernel characterizing the retrieval at a specific altitude returns the sensitivity of the retrieval at that altitude, i.e. to which extent the retrieval at that specific altitude comes from the spectral measurement rather than the apriori, while the sum of the averaging kernels indicates how the true state at a specific altitude changes the retrieved total column, i.e. the altitude to which the retrieved total column is mainly sensitive/representative.

Figure 3 (top and bottom panels) of Ronsmans et al. (2016) further presents the global distributions of the degrees of freedom for signal (DOFS, top panels) and of the altitude of maximum sensitivity of the retrieval to the HNO_3 profile (bottom panel), separately for January (left) and July (right) 2011, when the strong HNO_3 depletion occurs within the cold Antarctic winter. It clearly shows that above the Antarctic, the altitude of maximum sensitivity varies between ~9 km in summer and ~22 km in winter (~ 50 hPa) on average.

To address the comment of the referee without repeating too much of the earlier results, we have carefully verified the manuscript with regard to unclear or incomplete statements about vertical sensitivity. The following has been added in Section 1: "IASI provides reliable total column measurements of HNO3 with a maximum sensitivity in the low-middle stratosphere around 50 hPa (20 km) during the dark Antarctic winter (Ronsmans et al., 2016; 2018) …" and in Section 2: "… the largest sensitivity of IASI in the region of interest, i.e. in the low and mid-stratosphere (from 70 to 30 hPa), where the HNO_3 abundance is the highest (Ronsmans et al., 2016).

In order to convince the referee that IASI measurements capture the expected variations of HNO_3 within the polar night, we provide in Figure 1 below examples of vertical HNO_3 profiles retrieved within the dark Antarctic vortex (above Arrival Height) and outside the vortex (above Lauder). The retrieved profiles are shown along with their associated total retrieval error and averaging kernels (the total column AvK and the so-called "sensitivity profile" are also represented). Above Arrival Height during the dark Antarctic winter, we clearly see depleted HNO_3 levels in the low and mid-stratosphere and the altitude of maximum sensitivity at around 30 hPa. At Lauder on the contrary, HNO_3 levels larger than the a priori are observed in the stratosphere with a larger range of maximum sensitivity.

Specific comments

[L2: "good vertical sensitivity" ... only column HNO3 measurements are discussed here - there is no vertical resolution in the measurements.]
See our response to the second general comment above.

As stated in the text, we here refer to "a good vertical sensitivity in the low and middle stratosphere", not to a good vertical resolution of the measurement. Note that HNO_3 vertical profile are retrieved from IASI measurements, not simply total columns; Hence, even if the sensitivity covers the entire altitude range from the troposphere to the stratosphere with no clear decorrelation (poor resolution) between the retrieved layers forcing us to consider a total column, it is shown to variate with the altitude and to be highest in the low-middle stratosphere, which means that the variability in the measured total column is mainly representative of that layer.

As mentioned in the manuscript, this paper builds on the previous studies of Ronsmans et al. (2016) and (2018), where the vertical sensitivity of IASI to HNO_3 measurements is shown to be highest in the low and mid-stratosphere, even within the cold Antarctic polar vortex, with the degrees of freedom for signal (DOFS) that ranges from 0.9 to 1.2 at all latitudes. Note also that similarly to these two previous studies, HNO_3 measurements characterized by a poor spectral fit or by a low vertical sensitivity (DOFS < 0.9) have been filtered out of this analysis. This is now clearly mentioned in Section 2 of the revised manuscript:

"Quality flags similar to those developed for O_3 in previous IASI studies (Wespes et al., 2017) were applied a posteriori to exclude data (i) with a corresponding poor spectral fit (e.g. based on quality flags rejecting biased or sloped residuals, fits with maximum number of iteration exceeded), (ii) with less reliability (e.g. based on quality flags rejecting suspect averaging kernels, data with less sensitivity characterized by a DOFS lower than 0.9) or (iii) with tropospheric cloud contamination (defined by a fractional cloud cover larger than 25 %)."

[L10: 191K is also consistent with STS temperatures (192 K) and is actually closer than TNAT (195 K)]
Indeed but as stated in the manuscript: "… recent observational and modelling studies have shown that HNO_3 starts to condense in early PSC season in liquid NAT mixtures well above Tice (~4 K below T_{NAT}, close to T_{STS})…". The NAT nucleation temperature at 50 hPa range from slightly below T_{NAT} to around 3-4 K below Tice, depending on atmospheric conditions, on TTE and on the type of formation mechanisms (Pitts et al., 2011; Peter and GrooS, 2012; Hoyle et al., 2013).

Note that in replying to referee#1 we have identified a bug for the automatically detection of the drop temperature, as well as for the detection of the corresponding dates in the figure 2 of the manuscript. It has been corrected. The position of the drop temperatures does now perfectly match the yearly minima of the total HNO_3 second derivative. An average drop temperature over the ten years of IASI of 194.2 +/- 3.8 K is now calculated, which is even closer to T_{NAT}.

Finally, as requested by referee #1, we also now clearly mention in Section 4.1 of the manuscript the range of drop temperatures when calculated at two other pressure levels to better judge on the uncertainty of the drop temperature at 50 hPa (see Figure 3 here below):

"… Nevertheless, given the range of maximum IASI sensitivity to HNO_3 around 50 hPa, typically between 70 and 30 hPa (Ronsmans et al., 2016), the drop temperatures are also calculated at these two other pressure levels (not shown here) to estimate the uncertainty of the calculated drop temperature defined in this study at 50 hPa. The 30 hPa and 70 hPa drop temperatures range respectively over 185.7 K – 194.9 K and over 194.8 K – 203.7 K, with an average of 192.0 +/- 2.9 K and 198.0 +/- 3.2 K (1σ standard deviation) over the ten years of IASI. The average values at 30 hPa and 70 hPa fall within the 1σ standard deviation associated with the average drop temperature at 50 hPa. It is also worth noting the agreement between the drop temperatures and the NAT formation threshold at these two pressure levels (T_{NAT} ~193 K at 30 hPa and ~197 K at 70 hPa) (Lambert et al., 2016)."

[L18: add more recent references e.g. Peter and Gross (2012). L28: Much more has been done in the past decade with MIPAS and CALIOP that should be referenced]
Thank you for this suggestion. Peter and GrooS (2012) was cited elsewhere in the manuscript but has been added here as well. Note that the goal of the introduction is not to provide an exhaustive list of all studies related to the PSC thermodynamics. Several general reference papers are cited and we have decided to put more focus here on HNO_3.

[L59: This section should explain what is meant by "maximum sensitivity" etc.]
See our responses to the second major comment and specific comments above.

[L79: Information on the data quality for IASI HNO3 is poor. Is the value of bias and uncertainty the same for depleted and non-depleted conditions?]
The reader is here invited to refer to the figure 4 of Ronsmans et al. (2016) which illustrates the global distribution of the total retrieval error for HNO_3 (integrated over 5 to 35 km) separately for January (left) and July (right) over the period of the IASI measurements. The mid- and polar latitudes are characterized by low total retrieval errors of around ~3-5% - which corresponds to a reduction by a factor of 18-30 compared to the prior uncertainty (90%) and indicates a real gain of information – except above Antarctica during wintertime where the errors reach 25%. They are explained by (1) a weaker sensitivity (i.e. a larger smoothing error which represents in all cases the largest source of the retrieval error) above such cold surface (DOFS of ~0.95 within the dark Antarctic vortex – see figure 3 of Ronsmans et al., 2016) and by (2) a poor knowledge of the wavenumber-dependent surface emissivity above ice surface, which also varies in time (Hurtmans et al., 2012).). This is made more explicit in Section 2 of the revised manuscript:

"The total columns are associated with a total retrieval error ranging from around 3% at mid- and polar latitudes to 25% above cold Antarctic surface during winter (due to a weaker sensitivity above very cold surface with a DOFS of ~0.95 and to an poor knowledge of the seasonally and wavenumber-dependent emissivity above ice surfaces which induces larger forward model errors), and a low bias (lower than 12%) in polar regions over the altitude range where the IASI sensitivity is the largest, when compared to ground-based FTIR measurements (see Hurtmans et al., 2012; Ronsmans et al., 2016)."

[L82: Yet, problems with the retrievals because of cloud contamination seem to remain even after the <25% cloud fraction filter is applied.]
We do not understand the referee comment here. In this section of the manuscript, we only describe the quality flags used in our analysis.

[L83: Cloud contamination? Tropospheric cloud only or also thick ice PSCs?]

The clouds that have most impact are clearly tropospheric water clouds. Cirrus clouds or PSCs are mostly transparent in the IR; thick cirrus however show up in the longwave part of the IASI spectrum, below 900 cm^{-1}. We have added “tropospheric cloud contamination” in the text.

Note that the threshold of 25 % cloud cover was carefully chosen after a series of tests, which have shown that these scenes could be treated as cloud-free without significant impact on the retrievals (Hurtmans et al., 2012).

[L102: Why was 2011 chosen?]
As expected from figure 1c, any other year could have been chosen instead of the year 2011 to illustrate the HNO_3 total columns versus temperatures (at 50 hPa) histogram in figure 1b. It is now clearly mentioned in the revised manuscript:

“Similar histograms are observed for the ten years of IASI measurements (not shown).”

[L106: Heterogeneous hydrolysis of N2O5 requires aerosol particles. So this process starts with cold binary aerosols (i.e. sulfates) before the formation of STS?]
Indeed, previous studies have shown enhanced HNO_3 columns during autumn in Antarctica and have attributed them to decreasing sunlight and conversion of N_20_5 to HNO_3 by the reaction of N_20_5 with background aerosols, before the formation of polar stratospheric clouds (e.g. Keys et al., Nature, 1993). At these temperatures, the conversion may occur on binary sulfuric aerosols.

The sentence has been rewritten as follows:

“These high HNO_3 levels result from low sunlight, preventing photodissociation, along with the heterogeneous hydrolysis of N_2O_5 to HNO_3 during autumn before the formation of polar stratospheric clouds (Keys et al., 1993; Santee et al., 1999; Urban et al., 2009; DeZafra et al., 2001). This period also corresponds to the onset of the deployment of the southern polar vortex which is characterized by strong diabatic descent with weak latitudinal mixing across its boundary, isolating polar HNO_3-rich air from lower latitudinal airmasses.”

[L129: The onset of depletion seems to start when the temperatures fall substantially below 190K from inspection of Fig 1(c) and quite far below the red line marked at 195K.]
The onset of HNO_3 depletion starts in June at around 190K, which is in agreement with figure 1a.

[L136-137: Why are two temperatures (180 and 185 K) quoted for 30hPa? Why is the actual value from Fig1(c) (I estimate this as about 188K) for the 50hPa temperature not given in L129?]
The sentence has been rewritten for clarity:
“The results (not shown here) exhibit a similar HNO_3-temperature behaviour at the different levels with, as expected, lower and larger temperatures in R2, respectively, at 30 hPa (down to 180 K) and at 70 hPa 145 (down to 185K), but still below the NAT formation threshold at these pressure levels (T_{NAT} =193 K at 30 hPa and 197 K at 70 hPa) (Lambert et al., 2016).”

[L138: "characterized by" seems the wrong description for the chance occurrence that the maximum sensitivity of IASI HNO3 falls in the same altitude range as the PSCs.]
Changed to: “… the altitude range of maximum IASI sensitivity to HNO_3 (see Section 2) is characterized by temperatures that are below the NAT formation threshold at these pressure levels, enabling the PSCs formation and the denitrification process.”

[L139-146: This section rather seems to belong in the conclusions.]

L150-154 of the revised manuscript has been moved to the conclusions.

[L148: Clearly this does not "go beyond the vertically integrated view" since the column HNO3 is all that is available. It could be reworded as "To identify the spatial and temporal variability of the column HNO3 ..."]

Corrected as suggested.

[L165-169: Denitrification is the term used to describe the permanent removal of some HNO3 from the gas phase by sedimentation of PSCs. Sequestration is the term used to describe the uptake of HNO3 from the gas phase into PSCs. Denitrification by STS is a lengthy process compared to NAT since the smaller STS particles sediment slowly. STS can (and frequently does) form without the prior nucleation of NAT. IASI alone cannot discriminate between these processes and it should not be assumed that what is observed is the "onset of HNO3 denitrification".]

We thank the referee for this remark. We are of course aware of the definition of the so-called “denitrification”. We agree that, from IASI, we can only measure a “removal from the gas phase”, caused by sequestration into particles with or without sedimentation. Careful attention has now been made in the manuscript to avoid abusive use of the term “denitrification”. Hence, “onset of HNO_3 denitrification” has been changed to “the onset of HNO_3 depletion” in L.169 and where appropriated in the revised manuscript and he title has also been changed accordingly to:

“Polar stratospheric HNO_3 depletion surveyed from a decadal dataset of IASI total columns”.

[L185-187: 210K is much too high for PSC formation, but could possibly be NAT that is in process of melting? If these are observed over ocean then they warrant further investigation. However, why are specific regions with emissivity features not flagged as such? They should be discarded rather than "used with caution".]

Bright land surface such as desert or ice might in some cases lead to poor HNO_3 retrievals due to a poor knowledge of the wavenumber-dependent emissivity above such surfaces, which can alter the retrieval by compensation effects (Wespes et al., 2009). FORLI relies on the monthly climatology of surface emissivity built by Zhou et al. (2011) from several years of IASI measurements on a 0.5x0.5 grid and for each 8461 IASI spectral channels when available, or on the MODIS climatology that is unfortunately restricted to only 12 channels in the IASI spectral range; see Hurtmans et al. (2012) for more details. Although wavenumber-dependent surface emissivity atlases are used in FORLI, it is clear that this parameter remains critical and causes poorer retrievals that, in some instances, pass the posterior filtering. The total HNO_3 columns over eastern Antarctica which show drop temperatures much above 195K might precisely be related to this. We have made this clear in Section 4.2 of the revised version:

“…emissivity features that are known to yield errors in the IASI retrievals. Indeed, bright land surface such as ice might in some cases lead to poor HNO_3 retrievals. Although wavenumber-dependent surface emissivity atlases are used in FORLI (Hurtmans et al., 2012), this parameter remains critical and causes poorer retrievals that, in some instances, pass through the series of quality filters and could affect the drop temperature calculation.”

We refer on the good agreement with MLS (suggested by the referee) to underline the potentiality of IASI to detect the HNO_3 variations as well within the Antarctic winter (see general comment and Figure 1 here below).

[L189: Modern reanalysis temperatures (e.g. ERA-I) do not "feature large uncertainties" large enough to account for a 195K to 210K shift. L195-L201: The limitations of the reanalysis temperatures seems to be an accuracy of better than 1K and clearly this in no way limits the derivation of the "50hPa drop temperature" which simply necessitates finding the 50hPa reanalysis temperature that corresponds to the second derivative wrt time minimum in column HNO3.]

We agree with the referee's comment; the discussion about the potential role of the uncertainty of the ECMWF reanalysis temperature on the drop temperature has been removed from the section, hence, this paragraph has been strongly revised accordingly:

"… while biases in ECMWF reanalysis are too small for explaining the spatial variation in drop temperatures. Thanks to the assimilation of an advanced Tiros Operational Vertical Sounder (ATOVS) around 1998–2000 in reanalyses, to the better coverage of satellite instruments and to the use of global navigation satellite system (GNSS) radio occultation (RO) (Schreiner et al., 2007; Wang et al., 2007; Lambert and Santee, 2018; Lawrence et al., 2018), the uncertainties have been vastly reduced. Comparisons of the ECMWF ERA Interim dataset used in this work with the COSMIC data (Lambert and Santee, 2018) found a small warm bias, with median differences around 0.5 K, reaching 0–0.25 K in the southernmost regions of the globe at ~68–21 hPa where PSCs form."

[What is meant by "spatial variability"? The plots in Fig 5 show the spatial distribution of the drop temperature over a number of years but what variability is being considered? Interannual? Why have these spatial maps of drop temperatures not been compared with published maps of PSC types made by CALIOP or MIPAS. Wouldn't some correlation be expected according to the arguments made here? i.e. NAT PSCs at the higher temperature e.g. the highest temperatures (orange) appear downstream of the Palmar Peninsula in the "NAT ring" structure described by Hopfner et al (2006).]

Corrected: "Figure 5 shows the spatial variability" → "Figure 5 shows the spatial distribution".

We do not understand the referee's comment here. Figure 5 of the manuscript shows the spatial distribution of the drop temperature calculated inside a region enclosed by an isocontour PV of $-8x10^{-5}$ $K.m^2.kg^{-1}.s^{-1}$, which, hence, encircles a region larger than the inner vortex core (see Figures 3 and 4 of the manuscript). The drop temperatures much above the NAT formation temperature, which are mostly found outside the averaged isocontour PV of $-10x10^{-5}$ $K.m^2.kg^{-1}.s^{-1}$, do not correspond to high minima (>-0.5 $x10^{14}$ $molec.cm^{-2}.d^{-2}$) in the second derivative of HNO_3 total column with respect to time. We cannot argue that it corresponds to the NAT belt of Höpfner et al. (2006) downstream of the Antarctic Peninsula, which was enclosed inside the region of the NAT threshold temperature; the highest drop temperatures from IASI are found on the contrary outside the isocontour of the NAT threshold temperature (see figure 5 of the revised manuscript). In addition, comparing the distributions of drop temperatures from IASI with PSC information from CALIPSO/MIPAS remain difficult given the difference in spatial coverage and, most importantly, the highly variable distribution of PSC types and of the NAT belt, temporally (daily) and spatially (Höpfner et al., 2006; Lambert et al., 2012).

Finally, in response to G. Manney and M. Santee, the contour of $-10\times10^{-5}K.m^2.kg^{-1}.s^{-1}$ based on the minimum PV encountered at 50 hPa over the 10 May to 15 July period as well as the isocontours of 195 K at 50 hPa for the averaged temperatures and the minima over the same period are also now represented in the revised Fig.5 and the distribution of the drop temperatures is much better described and explained in the revised version:

"The averaged isocontour of 195 K encircles well the area of HNO_3 drop temperatures lower than 195 K, which means that the bins inside that area characterize airmasses that experience the NAT threshold temperature during a long time over the 10 May – 15 July period. That area encompasses the inner vortex core (delimited by the isocontour of $-10\times10^{-5}K.m^2.kg^{-1}.s^{-1}$ for the averaged PV) and show pronounced minima (lower than -0.5 $x10^{14}$ $molec.cm^{-2}.d^{-2}$) in the second derivative of the HNO_3 total column with respect to time (not shown here), which indicate a strong and rapid HNO_3 depletion.

The area enclosed between the two isocontours of 195 K for the temperatures, the averaged one and the one for the minimum temperatures, show higher drop temperatures and weakest minima (larger than -0.5 x10^{14} molec.cm^{-2}.d^{-2}) in the second derivative of the HNO_3 total column (not shown). That area is also enclosed by the isocontour of -10×10^{-5}K.m^2.kg^{-1}.s^{-1} for the minimum PV, meaning that the bins inside correspond, at least for one day over the 10 May – 15 July period, to airmasses located at the inner edge of the vortex and characterized by temperature lower than the NAT threshold temperature. The weakest minima in the second derivative of total HNO_3 (not shown) observed in that area indicate a weak and slow HNO_3 depletion and might be explained by a short period of the NAT threshold temperature experienced at the inner edge of the vortex. It could also reflect a mixing with strong HNO_3-depleted and colder airmasses from the inner vortex core. The mixing with these "already" depleted airmasses could also explained the higher drop temperatures detected in those bins. Finally, note also that these high drop temperatures are generally detected later (after the HNO_3 depletion occurs, i.e. after the 10 May – 15 July period considered here – not shown), which supports the transport, in those bins, of earlier HNO_3-depleted airmasses and the likely mixing at the edge of the vortex."

[L205: Nothing has been presented that demonstrates PSC occurrence. For that you would need to compare to actual data on PSCs from CALIOP and/or MIPAS.]
Corrected: "PSCs occurrence" → "NAT formation temperature"

[L224: Again, the suspect data should be discarded because of the detrimental impact on the scientific analysis. Also, if you cannot manage to work out and apply adequate quality control to your own data then you have no reason to expect anyone else to do so.]
See our response to comment [L185-187] above.

[L230: "To the best of our knowledge, it is the first time that such a large satellite observational data set of stratospheric HNO3 concentrations is exploited to monitor the evolution HNO3 versus temperatures" In fact you cite several papers that have done exactly this, but let's take the one published over two decades ago by Santee et al (1999) titled "Six years of UARS Microwave Limb Sounder HNO3 observations : Seasonal, interhemispheric, and interannual variations in the lower stratosphere". https://doi.org/10.1029/1998JD100089. Not only does this paper compare HNO3 with UKMO temperatures we are referred to a more complete paper on this topic on p8241 ... "The correlation of the HNO3 behavior with temperature during this time period, and its implications for PSC phase and composition, is explored in detail by Santee et al (1998). I noticed that the outside edge of the "HNO3 collar region" at 465K was defined by these authors as inside the 0.25 x E-4 K m2 kg-1 s-1 PV contour. This seems at odds with the 1E-4 value that is used for the second derivative minimum calculation in this paper and seemingly places the boundary quite far equatorward. Santee et al (1998) also includes a description of the heterogeneous hydration of N2O5 that would be helpful in response to the question above on L106.]
We here simply refer to the unprecedented potential of IASI in terms of its exceptional spatial and temporal sampling. Ronsmans et al. (2018) also referred to the IASI dataset and correlations with temperature were done but in a lesser extent. In order to avoid overselling, the sentence has been rewritten:
"We show in this study that the IASI dataset allows capturing the variability of stratospheric HNO_3 throughout the year (including the polar night) in the Antarctic. In that respect, it offers a new observational means to monitor the relation of HNO_3 to temperature and the related formation of PSCs."

In this study, we use the PV fields taken from the ECMWF ERA Interim Reanalysis dataset at the potential temperature of 530 K (corresponding to ~20 km where the IASI sensitivity to HNO_3 is the highest), while Santee et al. (1998) considered 465K. We clearly see from Figures 3a and 4 of the manuscript that PV contours at -0.5e-4 K m2 kg-1 s-1 and at -0.8e-4 K m2 kg-1 s-1 encompass the so-called HNO_3 collar region. The PV value of -1e-4 K m2 kg-1 s-1 is used in this study to calculate the drop temperature based on the second derivative minimum as it clearly encompass the regions inside the inner polar vortex (see Figure 3a and 4 of the manuscript).

[L231: "It could constitute a new accurate climatological parameter that could be inserted in the PSCs classification schemes." The analysis presented does not support this statement. Specifically, how could the HNO3 column amount be used in a classification scheme?]
This sentence has been removed.

Technical comments:

L8: in [the] Antarctic
L53: Studies of HNO3 depletion and PSC formation predate the sensors named in the paragraph e.g. the Santee et al (1999) reference used UARS/MLS launched in 1991, measurement using balloons should have been be referenced here.
L108: extends
Figure 1 caption: Each figure title in 1(b) needs to state the year e.g. "January - December 2011 or put a label "2011" above the whole figure.
Figure 1 caption: 50 hpa => 50 hPa
Figure 1 caption: it is not clear to what 0.1E16 molec. cm-2. This low value is not even on the y-axis of the figures. Figures 1(a) and 1(c): Are the HNO3 and temperature structures (localized peaks and valleys) visible in the time series in 1(a) quite well correlated when plotted as a scatter diagram as in 1(c), but without the 7-day averaging?
L123: 7-day
L124 and Figure 1 caption: "in the range of" : only one value is given and not a range of values
L130: Supplementary material - this does not appear to be available from the ACP website.
L164: drop temperatures
Figure 3 caption: sumperimposed => superimposed
L170: Figures 3a and b
L171: three isocontour levels
L174: lines indicate
L200: It underlines ... What does "it" refer to? The subject of the previous sentence is "the spatial variability" but that has not been defined.
L201:critical denitrification phase
L205: to PSCs occurrence to PSCs ??
L240: "All authors contributed to the writting of the text and reviewed the manuscript."
writting => writing

All the technical comments have been corrected.

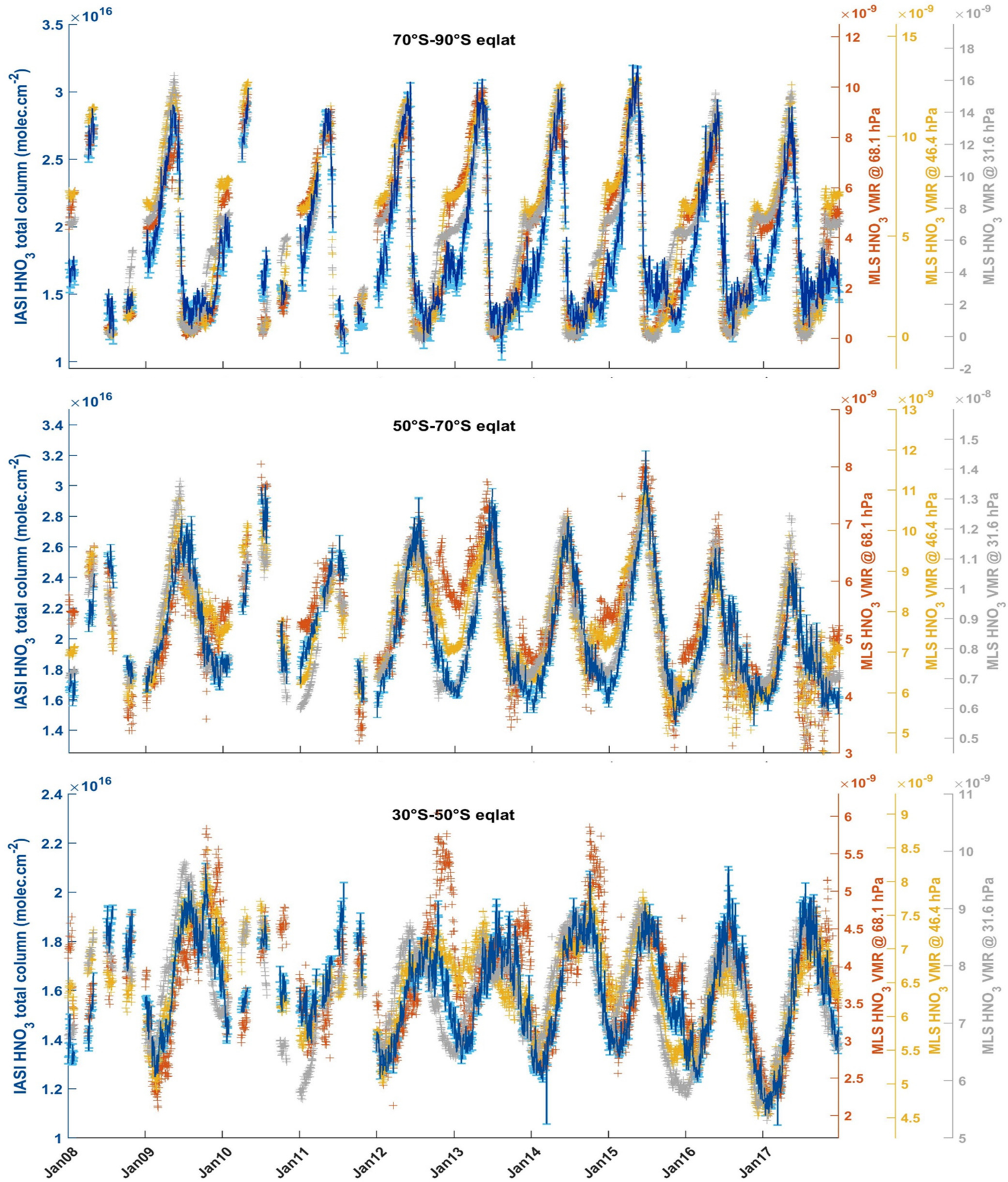

Figure 1. Time series of daily IASI total HNO_3 column (blue, left y-axis) co-located with MLS and of MLS VMR HNO_3 within 2.5x2.5 grid boxes at three pressure levels (at 30, 50 and 70 hPa; right y-axis), averaged in the 70°S–90°S (top panel), the 50°S–70°S (middle panel) and in the 30°S–50°S (bottom panel) equivalent latitude bands. The error bars (light blue) represents 3σ, where σ is the standard deviation around the IASI HNO_3 daily average.

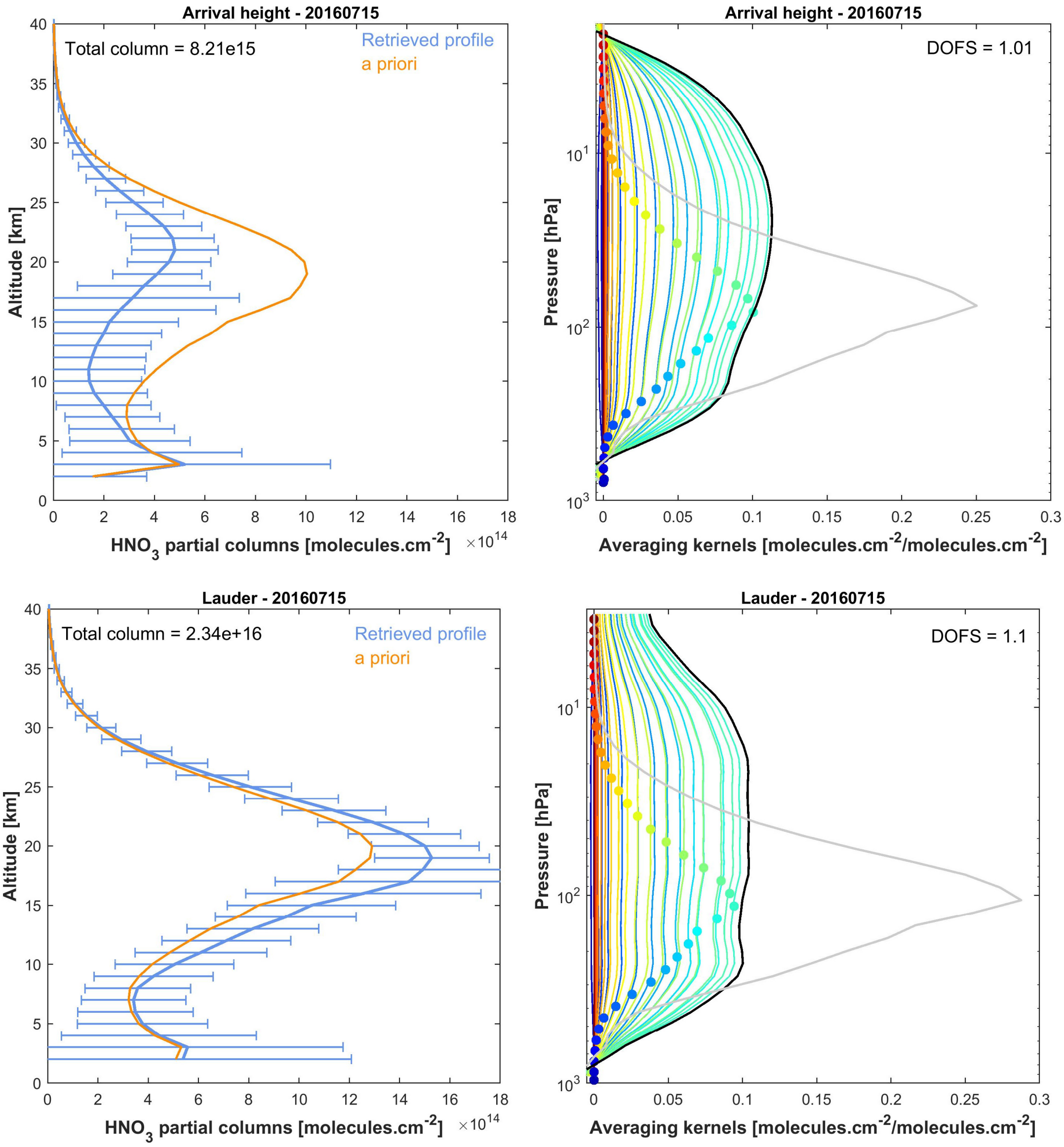

Figure 2. Examples of IASI HNO_3 vertical profiles (in molec.cm^{-2}) with corresponding averaging kernels (in molec.cm-^{2}/molec.cm-^{2}; with the total column averaging kernels (black) and the sensitivity profiles (grey)) above Arrival Height (77.49°S, 166.39°E, top panels) and Lauder (45.03°S, 169,40°E; bottom panels). The error bars associated with the HNO_3 vertical profile represent the total retrieval error. The a priori profile is also represented. The total column and the DOFS values are indicated.

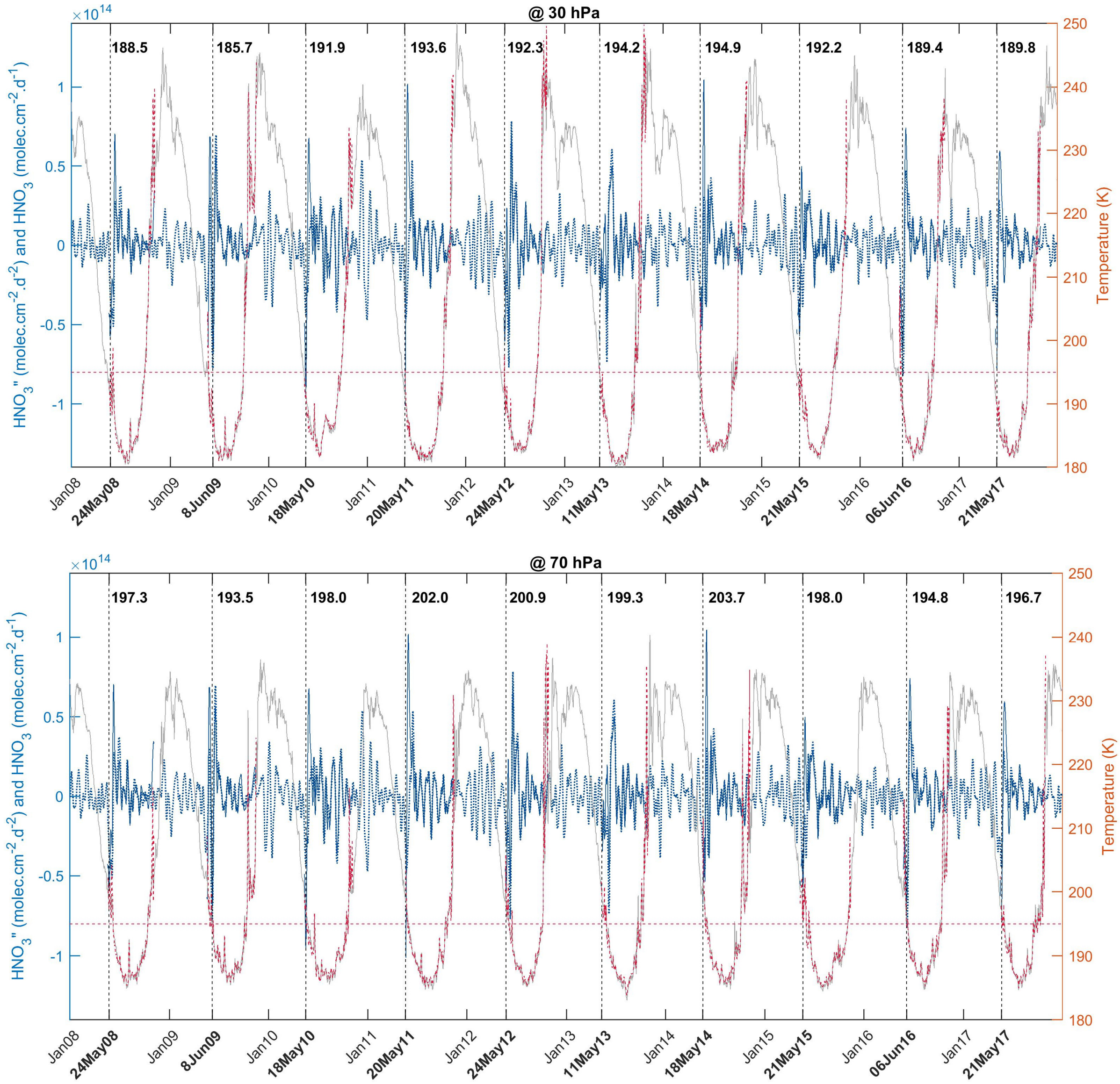

Figure 3. Time series of total HNO_3 second derivative (blue, left y-axis) and of the temperature (red, right y-axis) at 30 hPa (top panel) and 70 hPa (bottom panel), in the region of potential vorticity lower than -10 $x10^{-5}$ $K.m^2.kg^{-1}.s^{-1}$. The red horizontal line corresponds to the 195 K temperature. The vertical dashed lines indicate the second derivative minimum in HNO_3 for each year. The corresponding dates (in bold, on the x-axis) and temperatures are also indicated. The time series of total HNO_3 second derivative (dashed blue) and of temperature at 50 hPa (grey) in the70–90°S Eqlat band are also represented.

Response to Gloria Manney and Michelle Santee

We thank Gloria Manney and Michelle Santee for their extensive comments. Kindly find below our responses to each (quoted between []). We hope that our responses will clarify the main issues they have addressed. In particular, we hope that with the changes made, also in reply to the two anonymous reviewers, we have made more convincing that the IASI HNO_3 dataset has the potential to contribute to stratospheric studies in general, and to the time evolution of the polar processes in particular.

General comment

Throughout this manuscript, starting with its title, the term "denitrification" is taken to be synonymous with the uptake of gas-phase HNO3 through the formation of PSCs. Although not without precedent, this approach is contrary to common practice and may lead to confusion. Condensation of HNO3 in PSCs is usually referred to as "sequestration", while the term "denitrification" is usually reserved for the permanent removal of HNO3 from the lower stratosphere through the sedimentation of PSCs. In the absence of analysis of direct PSC measurements (e.g., from an instrument such as CALIOP), the occurrence of true denitrification can only be inferred from space-borne measurements of gaseous HNO3 when abundances do not rebound as PSCs dissipate at the end of winter, suggesting permanent removal. Thus the "drop temperature" derived in this study is indicative only of the onset of PSC formation, not the onset of denitrification, as is stated in numerous places in the paper.
We agree that, from IASI, we can only detect a "removal from the gas phase", caused by sequestration into particles with or without sedimentation. This misuse of the term "denitrification" was also highlighted by the two anonymous referees. Careful attention has been given in the manuscript to avoid abusive use of the term "denitrification". Hence, "onset of HNO_3 denitrification" has been changed to "the onset of HNO_3 depletion" in L.169 and where appropriate in the revised manuscript. The title has also been changed accordingly to:
"Polar stratospheric HNO_3 depletion surveyed from a decadal dataset of IASI total columns".

Specific comments

[Abstract: L2: It is misleading (particularly for those who read only the abstract of the paper) to characterize the IASI HNO_3 total columns as having "good vertical sensitivity". Indeed, this optimistic assessment is directly contradicted in Section 2, where IASI is stated to have "low vertical sensitivity ... with only one independent piece of information" (L76).]
As stated in the text, we here refer to "a good vertical <u>sensitivity in the low and middle stratosphere</u>", not to a good vertical <u>resolution</u> of the measurement. Note that HNO_3 vertical profiles are retrieved from IASI measurements, not simply total columns. Hence, even if the sensitivity covers the entire altitude range from the troposphere to the stratosphere with no clear decorrelation (DOFS~1) between the retrieved layers, it is shown in Ronsmans et al. (2016) that the highest sensitivity lies in the low-middle stratosphere, depending on latitude and season (from ~70 to 30 hPa within the cold Antarctic winter). This means that the variability in the measured total column is mainly representative of that layer. "low vertical sensitivity" in L76 has been changed to "low vertical resolution" to be more in line with the above.

We agree that the IASI sensitivity was insufficiently put forward in the text. We made it more explicit at several places in the revised manuscript; e.g. in Section 1: "IASI provides reliable total column measurements of HNO_3 characterized by a maximum sensitivity in the low-middle stratosphere around 50 hPa (20 km) during the dark Antarctic winter (Ronsmans et al., 2016; 2018) …" and in Section 2:

"… the largest sensitivity of IASI in the region of interest, i.e. in the low and mid-stratosphere (from 70 to 30 hPa), where the HNO_3 abundance is the highest (Ronsmans et al., 2016).

[Introduction: L48-49: It should be made more clear that this is by no means an exhaustive list of spaceborne instruments that have measured stratospheric HNO3.]
The study of Santee et al. (1999) on MLS/UARS measurements has been added:

"Several satellite instruments measure stratospheric HNO_3 (e.g. MLS/UARS (Santee et al., 1999), MLS/Aura (Santee et al., 2007), MIPAS/ENVISAT (Piccolo 50 and Dudhia, 2007), ACE-FTS/SCISAT (Sheese et al., 2017) and SMR/Odin (Urban et al., 2009))."

[Section 2: The information provided about the IASI HNO3 retrieval, data quality, and data screening is insufficient. This information is critical to assessing the robustness of the reported results, and readers should not be forced to refer to previous papers to find it.]
The reader is here invited to refer to the figure 4 of Ronsmans et al. (2016) which illustrates the global distribution of the total retrieval error for HNO_3 (integrated over 5 to 35 km) separately for January (left) and July (right) over the period of the IASI measurements. The mid- and polar latitudes are characterized by low total retrieval errors of around ~3-5% - which corresponds to a reduction by a factor of 18-30 compared to the prior uncertainty (90%) and indicates a real gain of information – except above Antarctica during wintertime where the errors reach 25%. They are explained by (1) a weaker sensitivity (i.e. a larger smoothing error which represents in all cases the largest source of the retrieval error) above such cold surface (DOFS of ~0.95 within the dark Antarctic vortex – see figure 3 of Ronsmans et al., 2016) and by (2) a misrepresentation of the wavenumber-dependent surface emissivity above ice surface (Hurtmans et al., 2012). As also required by the two anonymous referees, this is now made more explicit in Section 2 of the revised manuscript:

"The total columns are associated with a total retrieval error ranging from around 3% at mid- and polar latitudes to 25% above cold Antarctic surface during winter (due to a weaker sensitivity above very cold surface with a DOFS of ~0.95 and to an poor knowledge of the seasonally and wavenumber-dependent emissivity above ice surfaces which induces larger forward model errors), and a low bias (lower than 12%) in polar regions over the altitude range where the IASI sensitivity is largest, when compared to ground-based FTIR measurements (see Hurtmans et al., 2012; Ronsmans et al., 2016 for more details)."

Note also that similarly to these two previous studies, HNO_3 measurements characterized by a poor spectral fit or by a low information content (DOFS < 0.9) have been filtered out of this analysis. This is now clearly mentioned in Section 2 of the revised manuscript:

"Quality flags similar to those developed for O_3 in previous IASI studies (Wespes et al., 2017) were applied a posteriori to exclude data (i) with a corresponding poor spectral fit (e.g. based on quality flags rejecting biased or sloped residuals, fits with maximum number of iteration exceeded), (ii) with less reliability (e.g. based on quality flags rejecting suspect averaging kernels, data with less sensitivity characterized by a DOFS lower than 0.9) or (iii) with tropospheric cloud contamination (defined by a fractional cloud cover larger than 25 %)."

[In later sections (e.g., L186, L225), errors in IASI retrievals arising from issues with emissivity above ice shelves are invoked to account for some dubious results, but no mention of these poor-quality retrievals is made in the "Data" section, nor is it explained why quality-control measures fail to properly filter out these suspect data points.]
See our response to the above comment.

Bright land surface such as desert or ice might in some cases lead to poor HNO_3 retrievals due to a poor knowledge of the wavenumber-dependent emissivity above such surfaces, which can alter the retrieval by compensation effects (Wespes et al., 2009). FORLI relies on the monthly climatology of surface emissivity built by Zhou et al. (2011) from several years of IASI measurements on a 0.5x0.5 grid and for each 8461 IASI spectral channels when available, or on the MODIS climatology that is unfortunately restricted to only 12 channels in the IASI spectral range; see Hurtmans et al. (2012) for more details. Although wavenumber-dependent surface emissivity atlases are used in FORLI, it is clear that this parameter remains critical and causes poorer retrievals that, in some instances, pass the posterior filtering. The total HNO_3 columns over eastern Antarctica which show drop temperatures much above 195K might precisely be related to this. We have made this clear in Section 4.2 of the revised version:

"…emissivity features that are known to yield errors in the IASI retrievals. Indeed, bright land surface such as ice might in some cases lead to poor HNO_3 retrievals. Although wavenumber-dependent surface emissivity atlases are used in FORLI (Hurtmans et al., 2012), this parameter remains critical and causes poorer retrievals that, in some instances, pass through the series of quality filters and could affect the drop temperature calculation."

[L78: 10 km can hardly be characterized as the "mid-stratosphere".]
It has been corrected:
"… in the low and mid-stratosphere (from ~70 to ~30 hPa),…"

[L84: "normal" has a specific statistical meaning and is not the appropriate word here.]
The reviewers are right; "normal" has been removed.

[L85-86: The validity of the analysis approach depends on the 50 hPa pressure surface and the 530 K isentropic surface being in very close proximity during Antarctic winter. This implicit assumption should be explicitly justified in the paper.]
Figure 1 below represents the figure 2 of the manuscript but for the temperature at 30 hPa (top panel) and 70 hPa (bottom panel) for the sake of comparison. As expected, the drop temperatures are the lowest when using the temperatures at 30 hPa. They vary from 185-195 K (~192K on average) at 30 hPa to 195-204 K (~198 K on average) at 70 hPa with values of ~189-202 K (~194 K on average) at 50 hPa. As explained in the manuscript, the use of the 195 K at 50 hPa as single level for the analysis is justified by the fact that it corresponds best to the maximum of IASI vertical sensitivity during the polar night (see Figure 3 of Ronsmans et al. 2016 and responses to related comments above); another justification is found a posteriori by the consistency between the 195 K threshold temperature taken at 50 hPa and the onset of the strong total HNO_3 depletion seen by IASI, which matches the NAT development that occurs in June around that level. However, we fully agree that the HNO_3 abundances over a large part of the stratosphere (between 70 and 30 hPa) contribute to the total HNO_3 variations detected by IASI and that this inevitably affects the drop temperature calculation at 50 hPa. In order to address this issue and as also requested by referee #1, we have added in the manuscript the range of drop temperatures when calculated at these two other pressure levels (from 185 K to 204 K); this indeed allows the reader to better judge on the uncertainty of the drop temperature at 50 hPa (189-202 K). The text in the revised manuscript is changed to:
"… Nevertheless, given the range of maximum IASI sensitivity to HNO_3 around 50 hPa, typically between 70 and 30 hPa (Ronsmans et al., 2016), the drop temperatures are also calculated at these two other pressure levels (not shown here) to estimate the uncertainty of the calculated drop temperature defined in this study at 50 hPa. The 30 hPa and 70 hPa drop temperatures range respectively over 185.7 K – 194.9 K and over 194.8 K – 203.7 K, with an average of 192.0 +/- 2.9 K and 198.0 +/- 3.2 K (1σ

standard deviation) over the ten years of IASI. The average values at 30 hPa and 70 hPa fall within the 1σ standard deviation associated with the average drop temperature at 50 hPa. It is also worth noting the agreement between the drop temperatures and the NAT formation threshold at these two pressure levels (T_{NAT} ~193 K at 30 hPa and ~197 K at 70 hPa) (Lambert et al., 2016)."

See comment here below for the justification of a single theta level (530 K) for the PV.

[L89-91: It is highly problematic to use a single theta level to distinguish inside from outside vortex regions for column measurements. This approach implicitly (and erroneously) assumes that the vortex does not tilt, shrink, or expand with height over the altitude range considered. A better approach would have been to check PV over a range of levels and discard measurements classified as outside the vortex at any one of those levels. A similar comment can be made concerning the use of a single pressure level for temperature. Again, it might have been better to use a range of T over the ~10–30 km layer where IASI has most sensitivity. Some attempt is made to justify the latter choice (using 195 K at 50 hPa) in Section 3 (L141-142) and Section 4 (L168-169), but the arguments are not convincing, as the authors themselves appear to recognize when they state (L188-189) "hence, the use of temperature at a single pressure level might be restrictive to some extent".]
Here again, the approach that we have followed was to select the levels that correspond best to the altitude of IASI maximum vertical sensitivity during the polar night (see Figure 3 of Ronsmans et al. 2016 and responses to related comments above). We agree, however, that considering PV over the range of the largest IASI sensitivity (from ~30 to ~70 hPa during the polar night) would allow the reader to better judge on the uncertainty of our approach. To that end, the figure 2 below compares the maps of PV at 475 K (~65 hPa), 530 K (~50 hPa) and 600 K (~30 hPa) over the southern latitudes averaged over the period 15 May – 15 July (period of drop temperatures detection inside the inner vortex core) for the year 2008. They show quite similar shape of the vortex over the altitude of maximum IASI sensitivity which, hence, has only small influence on our delimitation of the inner polar vortex (delimited by a PV value of $-10\times10^{-5} K.m^2.kg^{-1}.s^{-1}$ at 530 K) and, thus, on the detection of the drop temperature averaged inside that region (see Figure 2 of the manuscript). Note, furthermore, that our approach has no influence on the spatial distribution of the drop temperature illustrated in Fig.5 of the manuscript, which is independent of the PV.

See comment here above for the justification of the use of a single pressure level (50 hPa) for the temperature.

[Section 3: The definition of the three "regimes" in the T/HNO3 relationship seems arbitrary and not well justified. For example, R1 is defined to begin in April, but Fig. 1a shows that HNO3 values start to increase rapidly and temperatures start to decrease rapidly in March (or even February, as noted in L117), not April. Only R2 encompasses a steep change in HNO3, but that regime also includes a lengthy period during which HNO3 remains nearly constant. It might have been better to break R2 into an "onset of PSC formation" phase and a "denitrification plateau" phase. Moreover, as defined in the paper, R2 extends through, not to, September as stated in L108. These problems are evident in the discussion in this section, as in some cases the behavior ascribed to one regime actually occurs in another.]
The definition of the three "regimes" in the T/HNO_3 relationship made here is actually based on changed in both HNO_3 and T, not only in HNO_3.

We did not stated in our manuscript that "HNO_3 values start to increase rapidly and temperatures start to decrease rapidly in March (or even February, as noted in L117), not April". In the manuscript, it is clearly stated in L117: "The plateau lasts until approximately February, where HNO_3 total column slowly starts increasing, reaching the April-May maximum in R1". Our statement specifically justified the start of R1 in April.

We changed "R2 extends from June to September" to "R2 extends from June to October" in L108.

[L102 and Fig. 1 caption: The red line in Fig. 1a is horizontal, not vertical, and Fig. 1b contains no such line – it is on Fig. 1c. Neither red line is defined in the caption.]
For Fig.1a: "horizontal" has been changed to "vertical".
Fig. 1b and 1c do contain a red vertical line.
The red horizontal or vertical lines are now mentioned in the caption of the revised manuscript.

[L102 and Fig. 1: 2011 was a particularly cold and long-lasting Antarctic winter, and thus it is arguably not representative. Some explanation for why that year was selected for highlighting in Fig. 1b is needed.]
As expected from figure 1c, any other year could have been chosen instead of the year 2011 to illustrate the HNO_3 total columns versus temperatures (at 50 hPa) histogram in figure 1b. It is now clearly mentioned in the revised manuscript:
"Similar histograms are observed for the ten years of IASI measurements (not shown)."

[L105-106: The contribution of confined descent inside the developing vortex bringing air rich in HNO3 from above into the domain where IASI is most sensitive has been ignored here – isn't descent also a factor leading to the observed high HNO3 total column values in early austral autumn?]
The domain where IASI is the most sensitive does actually cover the maximum HNO_3 concentrations, hence, the high HNO_3 total column values cannot be explained by the descent of HNO_3 rich air.

However, in response to the two anonymous referees, the sentence has been rewritten as follows:

"These high HNO_3 levels result from low sunlight, preventing photodissociation, along with the heterogeneous hydrolysis of N_2O_5 to HNO_3 during autumn before the formation of polar stratospheric clouds (Keys et al., 1993; Santee et al., 1999; Urban et al., 2009; DeZafra et al., 2001). This period also corresponds to the onset of the deployment of the southern polar vortex which is characterized by strong diabatic descent with weak latitudinal mixing across its boundary, isolating polar HNO_3-rich air from lower latitudinal airmasses."

[L115-116: In addition to a lack of citations of earlier papers on renitrification of the lowermost stratosphere (LMS), this sentence is not a very clear expression of the fact that IASI is not sensitive to the LMS and hence renitrification has little impact on the observed evolution of total column HNO3.]
The renitrification at lower stratospheric layers was merely mentioned here and it was not meant to be extensively reviewed. To address the comment, Lambert et al. (2012) , which was already cited at several places of the manuscript has been added here. It is clearly stated in the revised version that a likely renitrification of the LMS could hardly be detected given the maximum sensitivity of IASI to HNO_3 at higher levels than those at which it occurs:

"The likely renitrification of the lowermost stratosphere (Braun et al., 2019; Lambert et al., 2012), where the HNO_3 concentrations and the IASI sensitivity to HNO_3 are lower (Ronsmans et al., 2016), cannot be inferred from the IASI measurements."

[L119-121: Why is 2010 highlighted in Fig. 1a (green line)? Other recent Antarctic winters were also disturbed with some minor SSW activity, e.g., 2012 and 2013. Did those episodes not affect the HNO3 distribution? Also, why does the green line show T at 20 hPa, when the other curves show T at 50 hPa? More explanation for why the authors chose to show this particular level for this particular year is needed.]

As explained in the text, 2010 is chosen because of its highest HNO_3 levels and highest temperatures within the Antarctic winter. No strong warming and related enhanced HNO_3 levels are observed from IASI for the years 2012 and 2013 (see Fig. 2a and Fig.5 of the revised manuscript). We have chosen to illustrate the temperature at 20 hPa for 2010 (dotted green line) in addition to the ones at 50 hPa (dashed lines) for each year simply because that level shows a distinct increase in temperature (cfr de Laat and van Weele, 2011) reflecting the presence of a SSW during the winter of 2010, while at 50 hPa, the increase in temperatures is smaller (dashed green line).

[Fig. 1c: In general this plot is not well explained or well motivated. By showing the position in temperature / HNO3 space of the bin with the maximum number of observations, important information about the range of those values on a given day is omitted. The ranges in Fig. 1b suggest that the values at a given time may span most of the HNO3 axis in Fig. 1c, rendering the curves shown less meaningful. In addition, it is stated (L127) that this figure highlights the interannual variability in total HNO3, but interannual variability is also clearly seen in panel (a), which is much easier to interpret. The discussion relates the picture in Fig. 1c to the three regimes, but since they are not marked on this panel, it cannot easily be examined without reference to Fig. 1a. It is therefore not obvious what additional value this figure brings to the paper.]

We agree that figure 1c does not bring additional information in comparison with the figures 1a and 1b; however, it is an original way to give insight into the HNO_3/temperature cycle and, in that respect, it nicely complements figure 1a. We would not be in favour of removing it.

Regarding the other comment, it is true that the daily range of HNO_3 values around those of highest occurrence is not represented in Fig. 1c but note that it does not correspond to the range of HNO_3 values in Fig.1b which cover 3 months of IASI measurements. Hence, we do not agree with the comments that "The ranges in Fig. 1b suggest that the values at a given time may span most of the HNO_3 axis in Fig. 1c, rendering the curves shown less meaningful". The daily variability associated with the HNO_3 time series in the equivalent latitude bands can be found in Ronsmans et al. (2018).

In order to respond to the comment, the three regimes that were identified in Fig. 1a and Fig. 1b are now also indicated in Fig. 1c of the revised manuscript.

[L125: HNO3 columns are said to slowly increase as the T decreases over "February to May, i.e., R3 to R1". However, R3 is defined to start in October, and actually the slow increase in total HNO3 starts before February, arguably even as early as December.]

Here again we would like to stress that we did not only consider the change in HNO_3, but well the changes in both HNO_3 and temperature; HNO_3 columns do indeed increase as the temperature decrease over February to May but, before February, the HNO_3 levels increase as temperature also increase.

[L126: In the discussion of strong and rapid HNO3 depletion, "June (R1-R2)" should be "June-August (R2)".]

We indicate in the revised version: "… the strong and rapid HNO_3 depletion occurring in June (R2)"

[Section 4: Fig. 2 and its caption: More should be said about the agreement (or lack thereof) between the dashed and solid HNO3 and the grey and red T lines when they both exist. Some readers may question why the PV approach is used, given the gaps in those curves. Also, perhaps this is just an optical illusion, but the solid blue line appears to be thicker in some years (2011, 2014, 2016, 2017) than in the others.

If that is the case, then that also needs to be explained. In the caption, the level to which the stated PV value pertains (presumably 530 K) should be specified.]

The PV approach is indeed preferred for the calculation of the drop temperatures and the corresponding dates because it better delimits the inner vortex core. The time series in the 70–90°S Eqlat band are only represented for consistency with Fig.1a (Fig. 2a of the revised manuscript). Even if the time series in the PV isocontour of -10×10^{-5}K.m^2.kg^{-1}.s^{-1} or in the 70–90°S Eqlat band are very close during the Antarctic winter, differences in the drop temperature calculation might be found.

Only one blue solid line is plotted, hence, its width is the same over the IASI period.

The potential temperature at which the PV is taken (530 K) is now mentioned in the caption of the revised manuscript.

[L155: It is not appropriate to characterize the total HNO3 depletion in the inner vortex as being the “coldest”.]

Indeed a word was missing here. It has been corrected: “… the regions inside the inner polar vortex where the temperatures are the coldest and the total HNO_3 depletion occurs.”

[L160: The wording in this sentence is garbled.]

It has been rewritten for clarity: “Note that the HNO_3 time series has been smoothed with a simple spline data interpolation function to avoid gaps in order to calculate the second derivative of HNO_3 total column with respect to time as the daily second-difference HNO_3 total column”.

[L162-163: 23 is more than “a few” days.]

It has been changed to: “…within some days…”

[L174-179 and Fig. 3 caption: The description of the figure is confusing. It is stated in both in L174-175 and the caption that the vertical red dashed line indicates, at 90S, the 10-year average of the drop temperatures (191.1 K) calculated from the HNO3 second derivative time series in the area delimited by the −10×10-6 K.m2.kg-1.s-1 PV contour. It’s not clear how a vertical line on a time series plot can represent a temperature value. Perhaps the authors meant to say the average date on which T dropped below the 195 K threshold at 90S? Moreover, the discussion above indicated that the value of 191.1 K was the average for the inner vortex (defined by either PV or EqL), not specifically at the South Pole (90S). In addition, the scale for the PV contour should be 10-5, not 10-6. Then in L176-177, it is stated that the “delay of 4-23 days between the maximum in total HNO3 and the start of the depletion is also visible” – but how is a range of values (which arises from different years) visible in a climatological plot?]

The red dashed vertical line indeed represents the average drop temperature of 194.2 K calculated in the area delimited by the -10×10^{-5} K.m^2.kg^{-1}.s^{-1} PV contour; the position of the line matches the temperature of 194.2 K at 90°S. We agree that the representation of the averaged drop temperature is not clear. We now represent one isocontour for the averaged drop temperature and two vertical lines that encompass the dates on which the drop temperature is calculated. The scale for the PV contour has been corrected. We now state in the revised version that:

“The delay of some days between the maximum in total HNO_3 and the start of the depletion (see Fig. 3) is also visible in Fig. 4a.”

[Fig. 4: Very little discussion is devoted to this figure; it is merely noted (L177-178) that it shows the reproducibility of the IASI measurements of HNO3 depletion from year to year. Since Fig. 1 already makes this point, the added value of Fig. 4 is not clear.]

The figure 4 clearly illustrates the reproducibility, from year to year, of the edge of the collar HNO_3 region delimited by the PV isocontour of $-5\times10^{-5}K.m^2.kg^{-1}.s^{-1}$ and of the region of the strong HNO_3 depletion delimited by the PV isocontour of $-10\times10^{-5}K.m^2.kg^{-1}.s^{-1}$ taken at 50 hPa, the pressure level considered in this study to derive the drop temperatures. This cannot be inferred from Figure 1 and this is the main reason why we think that Figure 4 has to be kept.

[Fig. 5: How relevant is the PV contour averaged over the May to October period, when the dates of the onset of HNO3 depletion are May to June (or possibly July)? Why include August, September, and October in this average?]

We fully agree with that comment. Initially, the May-October period was chosen because it encompasses the dates of drop temperatures calculated in the region considered in Fig.5 (isocontour of $-8\times10^{-5}K.m^2.kg^{-1}.s^{-1}$). However, outside the polar vortex (defined by an isocontour of $-10\times10^{-5}K.m^2.kg^{-1}.s^{-1}$), drop temperatures are found much above the NAT formation temperature and they do not correspond to clear minima in the second derivative of HNO_3 total column with respect to time. Hence, considering that period for the PV contour is indeed not appropriate here.

We now represent, in the revised version, the PV contour over the 10 May to 15 July period that encompasses the dates of the onset of HNO_3 depletion inside the inner vortex core. Note that, on the contrary to the submitted version, we do not only consider the average of the PV over that period, but also the minima, which we find more representative of the drop temperature given the rapid displacement of the vortex: one bin can indeed be located inside the vortex one day and outside the vortex another day. Hence, that particular bin can be characterized by a depletion in HNO_3 with a specific drop temperature but an averaged PV larger than the value considered here to delimit the vortex core. The contour of $-10\times10^{-5}K.m^2.kg^{-1}.s^{-1}$ based on the minimum PV encountered over the 10 May to 15 July period as well as the isocontours of 195 K at 50 hPa for the averaged temperatures and the minima over the same period are also now represented in the revised Fig.5 and the distribution of the drop temperatures is much better described and explained in the revised version:

"The averaged isocontour of 195 K encircles well the area of HNO_3 drop temperatures lower than 195 K, which means that the bins inside that area characterize airmasses that experience the NAT threshold temperature during a long time over the 10 May – 15 July period. That area encompasses the inner vortex core (delimited by the isocontour of $-10\times10^{-5}K.m^2.kg^{-1}.s^{-1}$ for the averaged PV) and show pronounced minima (lower than -0.5 $x10^{14}$ $molec.cm^{-2}.d^{-2}$) in the second derivative of the HNO_3 total column with respect to time (not shown here), which indicate a strong and rapid HNO_3 depletion.

The area enclosed between the two isocontours of 195 K for the temperatures, the averaged one and the one for the minimum temperatures, show higher drop temperatures and weakest minima (larger than -0.5 $x10^{14}$ $molec.cm^{-2}.d^{-2}$) in the second derivative of the HNO_3 total column (not shown). That area is also enclosed by the isocontour of $-10\times10^{-5}K.m^2.kg^{-1}.s^{-1}$ for the minimum PV, meaning that the bins inside correspond, at least for one day over the 10 May – 15 July period, to airmasses located at the inner edge of the vortex and characterized by temperature lower than the NAT threshold temperature. The weakest minima in the second derivative of total HNO_3 (not shown) observed in that area indicate a weak and slow HNO_3 depletion and might be explained by a short period of the NAT threshold temperature experienced at the inner edge of the vortex. It could also reflect a mixing with strong HNO_3-depleted and colder airmasses from the inner vortex core. The mixing with these "already" depleted airmasses could also explained the higher drop temperatures detected in those bins. Finally, note also that these high drop temperatures are generally detected later (after the HNO_3 depletion occurs, i.e. after the 10 May – 15 July period considered here – not shown), which supports the transport, in those bins, of earlier HNO_3-depleted airmasses and the likely mixing at the edge of the vortex."

[L181: “the drop 50 hPa temperatures” should be “the 50 hPa drop temperatures”.]
It has been corrected.

[L183: Technically, the isocontour represents –10, not ≤ –10.]
It has been corrected.

[L184-185: First, how does the range of dates corresponding to the onset of HNO3 depletion reported here – mid-May to early July – relate to that reported (L163) in connection with Fig. 2, which was 17 May to 10 June? Does the difference in these estimates arise because the former is based on averages in 1°×1° bins, whereas the latter is based on a vortex average within the PV contour? July seems rather late for the onset of PSC formation. Similarly, the range in 50 hPa drop T is quoted as 188.2 K to 196.6 K in L164, whereas here drop Ts vary over a wider range, from 180 to 210 K. The values at both extremes of this range are unrealistic. Indeed, the date and T ranges found in connection with Fig. 5 call into question the analysis method.]
Indeed, the differences between the range in drop temperatures and corresponding dates shown in Fig.2 and in Fig.5 are simply due to the average (over the whole area delimited by a PV contour in Fig.2 vs in 1°x1° bins within the PV contour).
See our response to comment [L186, L225] above about the extreme unrealistic values of drop temperature: The total HNO_3 columns over eastern Antarctica which show drop temperatures much above 195K might precisely be contaminated by strong surface emissivity features above ice; We have made this clear in Section 4.2 of the revised version:
“…emissivity features that are known to yield errors in the IASI retrievals. Indeed, bright land surface such as ice might in some cases lead to poor HNO_3 retrievals. Although wavenumber-dependent surface emissivity atlases are used in FORLI (Hurtmans et al., 2012), it is clear that this parameter remains critical and causes poorer retrievals that, in some instances, pass through the series of quality filters and could affect the drop temperature calculation.”

[L189-196: The questionable results derived from this analysis cannot be pinned on biases in the ERA-Interim data. The statement is made that “Reanalysis data sets are, indeed, known to feature large uncertainties”, but the uncertainty in modern reanalysis temperatures (typically less than ~1 K) is by no means large enough to account for drop Ts as extreme as 180 and 210 K. The reliability of reanalysis temperatures in the polar lower stratosphere (including those from ERA-Interim) has been conclusively demonstrated in several recent papers, notably by Lawrence et al. [2018] and Lambert and Santee [2018]. Although both papers are cited here, their implications have apparently been overlooked.]
We fully agree with that remark that was also made by the referee #2. The discussion about the potential role of the uncertainty of the ECMWF reanalysis temperature on the drop temperature has been removed from the section, hence, this paragraph has been strongly revised accordingly:
“… while biases in ECMWF reanalysis are too small for explaining the spatial variation in drop temperatures. Thanks to the assimilation of an advanced Tiros Operational Vertical Sounder (ATOVS) around 1998–2000 in reanalyses, to the better coverage of satellite instruments and to the use of global navigation satellite system (GNSS) radio occultation (RO) (Schreiner et al., 2007; Wang et al., 2007; Lambert and Santee, 2018; Lawrence et al., 2018), the uncertainties have been vastly reduced. Comparisons of the ECMWF ERA Interim dataset used in this work with the COSMIC data (Lambert and Santee, 2018) found a small warm bias, with median differences around 0.5 K, reaching 0–0.25 K in the southernmost regions of the globe at ~68–21 hPa where PSCs form.”

[L197-199: This sentence is confusing and its intended meaning is unclear. It appears to be comparing apples (the spatial variability in drop T seen in the maps in Fig.5) to oranges (“natural” variations in PSC

nucleation T, TTE, and PSC formation mechanism). Perhaps the authors meant the spatial variability in those parameters (and not the values themselves), but that is not how the sentence is constructed. In any case, further discussion of comparisons of Fig. 5 with previously published results is warranted.]
We here simply link the range in drop temperatures with that in PSCs nucleation temperatures (explained by a series of parameters – atmospheric conditions, TTE, type of formation mechanisms), not the spatial variability. The sentence has been rewritten for clarity:

"Except above some parts of Antarctica which are prone to larger retrieval errors, the overall range in the drop 50 hPa temperature for total HNO_3, inside the isocontour for the averaged temperature of 195 K, typically extends from ~187 K to ~195 K, which fall within the range of PSCs nucleation temperature at 50 hPa …".

Furthermore, nota also that comparing the distributions of drop temperatures from IASI with PSC information from CALIPSO or MIPAS remains difficult given the difference in spatial coverage and, most importantly, the highly variable distribution of PSC types temporally (daily) and spatially (e.g. Höpfner et al., 2006; Lambert et al., 2012).

[L199-200: A number of other satellite data sets have captured gas-phase HNO3 depletion (from both sequestration and denitrification) on similarly large scales.]
Indeed and numerous references about HNO_3 measurements in the polar regions during winter are mentioned in the manuscript where appropriate.

[Conclusions: L225-226: It is stated that "the range of drop temperatures is interestingly found in line with the PSCs nucleation temperature that is known, from previous studies, to strongly depend on a series a factors". In fact, the derived range (180–210 K) is so large that it is arguably not in line with previous work, and it is therefore difficult to see how the IASI total column HNO3 measurements provide added value (as stated in L203) to studies of Antarctic PSC formation and the interannual variability therein beyond that obtained from other satellite HNO3 datasets.]
Please refer to our response to comment (L186, L225) above about the impact of the misrepresentation of the wavenumber-dependent surface emissivity above ice surface on the drop temperature calculation with some extreme values. Except for these extrema, the range of drop temperature is indeed in line with the PSCs nucleation temperature. This is now clearly mentioned in this section of the revised manuscript:

"Except for extreme drop temperatures that were found from year to year above eastern Antarctica and suspected to result from unfiltered poor quality retrievals in case of emissivity issues above ice, the range of drop temperatures is interestingly found in line with the PSCs nucleation temperature…"

[L230-231: The statement that this paper represents "the first time that such a large satellite observational data set of stratospheric HNO3 concentrations is exploited to monitor the evolution HNO3 versus temperatures" is wholly unsupportable. In fact, there is a substantial body of literature on the relationship between HNO3 and temperature, including studies of long-term vertically resolved datasets. In particular, Lambert et al. [2016] (which is cited in a number of places in this manuscript, but only inpassing) examined 10 years of Aura MLS HNO3 in the Antarctic winter vortex and its relationship to T – including temperature history (a factor that has been largely ignored here) and T with respect to TICE – as well as PSC composition as determined by CALIOP. In general, discussion of how the current results fit into the context of the findings from Lambert et al. [2016] and other relevant prior studies is inadequate.]

We wanted to highlight here the unprecedented exceptional spatial and temporal sampling of IASI for HNO_3 and certainly did not want to oversell the novelty of HNO_3-temperature correlations. The sentence has been rewritten:

"We show in this study that the IASI dataset allows capturing the variability of stratospheric HNO_3 throughout the year (including the polar night) in the Antarctic. In that respect, it offers a new observational means to monitor the relation of HNO_3 to temperature and the related formation of PSCs."

[L233-234: More explanation of how HNO3 total column amounts could be used to inform PSC classification schemes is needed to justify this statement, especially given how spatially heterogeneous and layered PSCs have been shown to be.]

This sentence has been removed.

[Finally, in addition to the serious substantive issues enumerated above and in the formal reviews of the official referees, the manuscript suffers from the poor quality of the writing. If this paper were to be eventually accepted for publication, it would require extensive copy-editing to improve the English.]

We hope that with the changes made in the revised manuscript, which now also includes a comparison with MLS, G. Manney and M. Santee will not go against publication. A detailed reading of the paper has been done to correct the English linguistic/grammar mistakes.

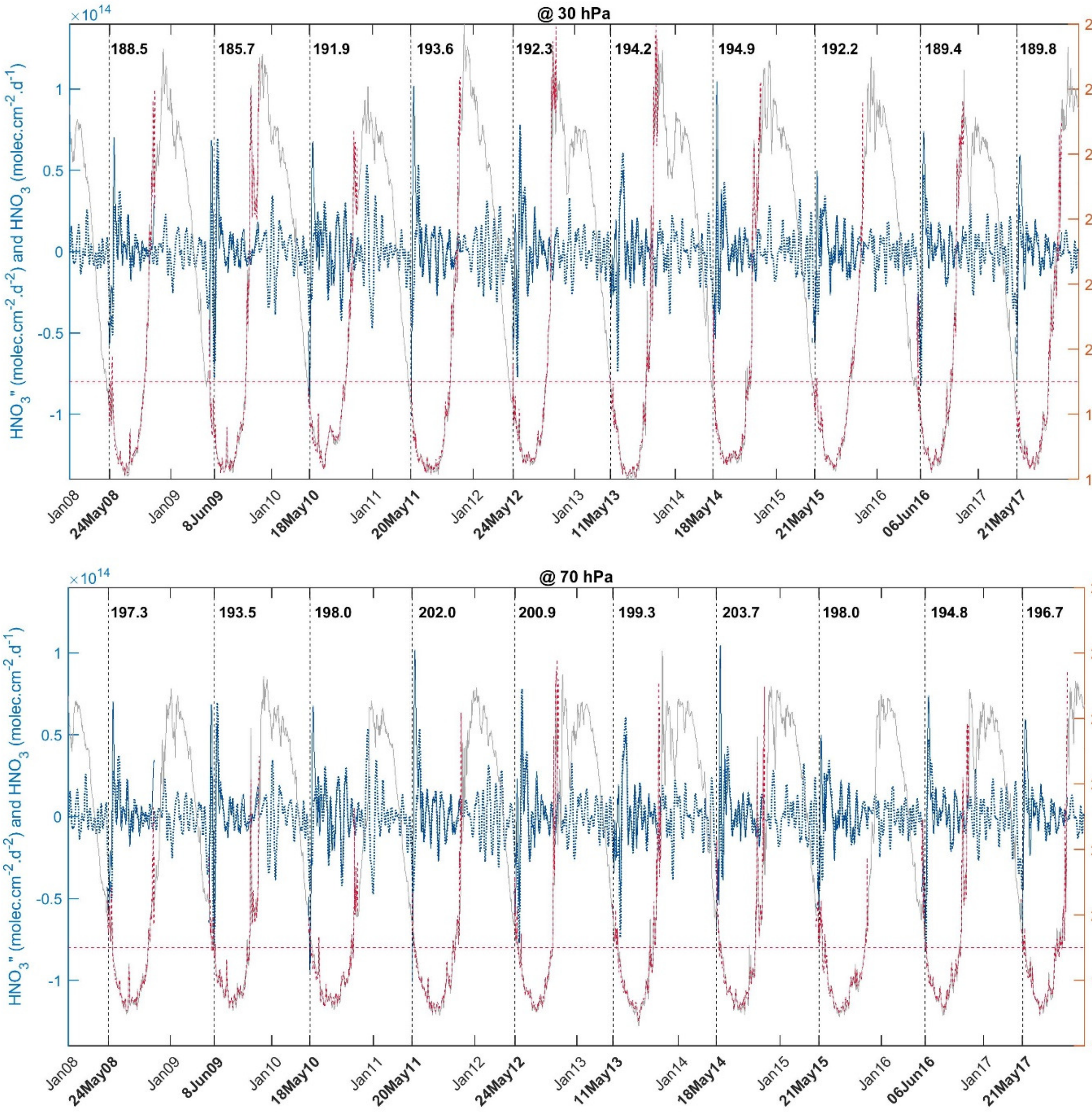

Figure 1. Same as Figure 2 of the manuscript but for the temperature at 30 hPa (top panel) and 70 hPa (bottom panel).

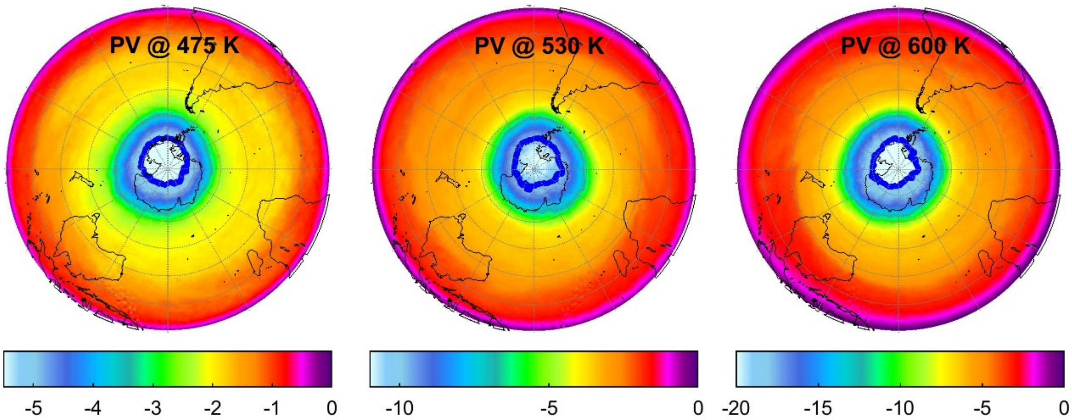

Figure 2. Spatial distribution of PV ($\times 10^{-5}$ K.m^2. kg^{-1}.s^{-1}) taken at three potential temperatures (475 K, 530 K and 600 K) over the range of the maximum IASI sensitivity, averaged over the period 15 May – 15 July for the year 2008. The blue lines represented the isocontours PV of -5.25×10^{-5} K.m^2. kg^{-1}.s^{-1} (at 475 K), -10×10^{-5} K.m^2. kg^{-1}.s^{-1} (at 530 K) and -19.4×10^{-5} K.m^2. kg^{-1}.s^{-1} (at 600 K) averaged over the considered period.

Polar stratospheric nitric acid depletion surveyed from a decadal dataset of IASI total columns

Gaetane Ronsmans[1], Catherine Wespes[1,*], Lieven Clarisse[1], Susan Solomon[2], Daniel Hurtmans[1], Cathy Clerbaux[1,3], and Pierre-François Coheur[1]

[1]Université libre de Bruxelles (ULB), Spectroscopy, Quantum Chemistry and Atmospheric Remote Sensing (SQUARES), Brussels, Belgium
[2]Department of Earth, Atmospheric and Planetary Sciences, Massachusetts Institute of Technology, Cambridge, Massachusetts, USA
[3]LATMOS/IPSL, Sorbonne Université, UVSQ, CNRS, Paris, France

Correspondence: Catherine Wespes (cwespes@ulb.ac.be)

Abstract

In this paper, we exploit the first 10-year data-record (2008-2017) of nitric acid (HNO_3) total columns measured by the IASI-A/Metop infrared sounder, characterized by an exceptional daily sampling and a good vertical sensitivity in the mid-stratosphere (around 50 hPa), to monitor the causal relationship between the temperature decrease and the observed HNO_3 loss that occurs each year in the Antarctic stratosphere during the polar night. Since the HNO_3 depletion results from the formation of polar stratospheric clouds (PSCs) which trigger the development of the ozone (O_3) hole, its continuous monitoring is of high importance. We verify here, from the 10-year time evolution of the pair HNO3-temperature (taken from reanalysis at 50 hPa), the recurrence of specific regimes in the cycle of IASI HNO_3 and identify, for each year, the day and the 50 hPa temperature ("drop temperature") corresponding to the onset of strong HNO_3 depletion in the Antarctic winter. Although the measured HNO_3 total column does not allow differentiating the uptake of HNO_3 by different types of PSC particles along the vertical profile, an average drop temperature of ~194.2 ± 3.8 K, consistent with the nitric acid trihydrate (NAT) formation temperature (close to 195 K at 50 hPa), is found in the region of potential vorticity lower than -10×10^{-5} $K.m^2.kg^{-1}.s^{-1}$. The spatial distribution and inter-annual variability of the drop temperature are ~~briefly~~ investigated and discussed in the context of previous PSCs studies. This paper highlights the capability of the IASI sounder to monitor the long-term evolution of the polar stratospheric composition and processes involved in the depletion of stratospheric O_3.

1 Introduction

The cold and isolated air masses found within the polar vortex during winter are associated with a strong denitrification of the stratosphere due to the formation of PSCs (composed of HNO_3, sulphuric acid (H_2SO_4) and water ice (H_2O)) (Peter, 1997; Voigt et al., 2000; von König, 2002; Schreiner et al., 2003; Peter and Grooß, 2012). These clouds strongly affect the polar chemistry by (1) acting as surfaces for the heterogeneous activation of chlorine and bromine compounds, in turn leading to enhanced O3 destruction (Solomon, 1999; Wang and Michelangeli, 2006; Harris et al., 2010; Wegner et al., 2012) and by (2) removing gas-phase HNO_3 temporarily or permanently through uptake by PSCs and sedimentation of large PSC particles to lower altitudes. The denitrification of the polar stratosphere during winter delays the reformation of chlorine reservoirs and, hence, intensifies the O_3 hole (Solomon, 1999; Harris et al., 2010). The heterogeneous reaction rates on PSCs surface and the uptake of HNO_3 strongly depend on the temperature and on the PSCs particle type. The PSCs are classified into three 3different types based on their composition and optical properties: type Ia solid nitric acid trihydrate -

NAT ($HNO_3.(H_2O)_3$), type Ib liquid supercooled ternary solution - STS ($HNO_3/H_2SO_4/H_2O$ with variable composition) and type II, crystalline water-ice particles (likely composed of a combination of different chemical phases) (Toon et al., 1986; Koop et al., 2000; Voigt et al., 2000; Lowe and MacKenzie, 2008). In the stratosphere, they mostly consist of mixtures of liquid/solid STS/NAT particles in varying number densities, with HNO_3 being the major constituent of these particles. The large-size NAT particles of low number density are the principal cause of sedimentation (Lambert et al., 2012; Pitts et al., 2013; Molleker et al., 2014; Lambert et al., 2016). The formation temperature of STS (T_{STS}) and the thermodynamic equilibrium temperatures of NAT (T_{NAT}) and ice (T_{ice}), have been determined, respectively, as: ~192 K (Carslaw et al., 1995), ~195.7 K (Hanson and Mauersberger, 1988) and ~188 K (Murphy and Koop, 2005) for typical 50 hPa atmospheric conditions (5 ppmv H_2O and 10 ppbv HNO_3). While the NAT nucleation was thought to require temperatures below T_{ice} and pre-existing ice particles, recent observational and modelling studies have shown that HNO_3 starts to condense in early PSC season in liquid NAT mixtures well above T_{ice} (~4 K below T_{NAT} , close to T_{STS}) even after a very short temperature threshold exposure (TTE) to these temperatures but also slightly below T_{NAT} after a long TTE, whereas the NAT existence persists up to T_{NAT} (Pitts et al., 2013; Hoyle et al., 2013; Lambert et al., 2016; Pitts et al., 2018). It has been recently proposed that the higher temperature condensation results from heterogeneous nucleation of NAT on meteoritic dust in liquid aerosol (Hoyle et al., 2013; Grooß et al., 2014; James et al., 2018). Further cooling below T_{STS} and T_{ice} leads to nucleation of liquid STS, of solid NAT onto ice and of ice particles mainly from STS (type II PSCs) (Lowe and MacKenzie, 2008). The formation of NAT and ice has also been shown to be triggered by stratospheric mountain-waves (Carslaw et al., 1998; Hoffmann et al., 2017). Although the formation mechanisms and composition of STS droplets in stratospheric conditions are well described (Toon et al., 1986; Carslaw et al., 1995; Lowe and MacKenzie, 2008), the NAT and ice nucleation processes still require further investigation. This could be important as the chemistry-climate models (CCMs) generally oversimplify the heterogeneous nucleation schemes for the PSCs formation (Zhu et al., 2015; Spang et al., 2018; Snels et al., 2019) preventing an accurate estimation of O_3 levels. The influence of HNO_3 in modulating O_3 abundances in the stratosphere is furthermore underrepresented in CCMs (Kvissel et al., 2012).

Several satellite instruments measure stratospheric HNO_3 (e.g. MLS/UARS (Santee et al., 1999), MLS/Aura (Santee et al., 2007), MIPAS/ENVISAT (Piccolo and Dudhia, 2007), ACE-FTS/SCISAT (Sheese et al., 2017) and SMR/Odin (Urban et al., 2009)). The spaceborne lidars CALIOP/CALIPSO and the infrared instrument MIPAS/Envisat) are capable to detect and classify the PSC types, and to follow their formation mechanisms (Lambert et al., 2016; Pitts et al., 2018; Spang et al., 2018) and references therein, which complements in situ measurements (Voigt et al., 2005) and ground-based lidar (Snels et al., 2019). From these available observational datasets, the HNO_3 depletion has been linked to the PSCs formation and detected below the T_{NAT} threshold (Santee et al., 1999; Urban 55 et al., 2009; Lambert et al., 2016; Ronsmans et al., 2018), but its relationship to PSCs still needs further investigation given the complexity of the nucleation mechanisms that depends on a series of parameters (e.g. atmospheric temperature, water and HNO_3 vapour pressure, time exposure to temperatures, temperature history).

In contrast to the limb satellite instruments mentioned above, the infrared nadir sounder IASI offers a dense spatial sampling of the entire globe, twice a day (Section 2). While it cannot provide a vertical profile of HNO_3 similar to the limb sounders, IASI provides reliable total column measurements of HNO_3 characterized by a maximum sensitivity in the low-middle stratosphere around 50 hPa (20 km) during the dark Antarctic winter (Ronsmans et al., 2016, 2018) where the PSCs cloud form (Voigt et al., 2005; Lambert et al., 2012; Spang et al., 2016, 2018). This study aims to explore the 10-years continuous HNO_3 measurements from IASI for providing a long-term global picture of depletion and of its dependence to temperatures during polar winter (Section 3). The temperature corresponding to the onset of the strong depletion in HNO_3 records (here referred to as 'drop temperature') is identified in Section 4 for each observed year and discussed in the context of previous studies.

2 Data

The HNO_3 data used in the present study are obtained from measurements of the Infrared Atmospheric Sounding Interferometer (IASI) embarked on the Metop-A satellite. IASI measures the Earth's and atmosphere's radiation in the thermal infrared spectral range (645 - 2760 cm^{-1}), with a 0.5 cm^{-1} apodized resolution and a low radiometric noise (Clerbaux et al., 2009; Hilton et al., 2012). Thanks to its polar sun-synchronous orbit with more than 14 orbits a day and a field of view of four simultaneous footprints of 12 km at nadir, IASI provides global coverage twice a day (9.30 AM and PM mean local solar time). That extensive spatial and temporal sampling in the polar regions is key to this study.

The HNO_3 vertical profiles are retrieved on a uniform vertical 1 km grid of 41 layers (from the surface to 40 km with an extra layer above to 60 km) in near-real-time by the Fast Optimal Retrieval on Layers for IASI (FORLI) software, using the optimal estimation method (Rodgers, 2000). Detailed information on the FORLI algorithm and retrieval parameters specific to HNO_3 can be found in previous papers (Hurtmans et al., 2012; Ronsmans et al., 2016). For this study, only the total columns (v20151001) are used, considering (1) the low vertical resolution of IASI with only one independent piece of information, (2) the limited sensitivity of IASI to tropospheric HNO_3, (3) the dominant contribution of the stratosphere to the HNO_3 total column and (4) the largest sensitivity of IASI in the region of interest, i.e. in the low and mid-stratosphere (from ~70 to ~30 hPa), where the HNO_3 abundance is the highest (Ronsmans et al., 2016). The total columns are associated with a total retrieval error ranging from around 3% at mid- and polar latitudes to 25% above cold Antarctic surface during winter (due to a weaker sensitivity above very cold surface with a DOFS of 0.95 and to an poor knowledge of the seasonally and wavenumber-dependent emissivity above ice surfaces which induces larger forward model errors), and a low bias (lower than 12%) in polar regions over the altitude range where the IASI sensitivity is the largest, when compared to ground-based FTIR measurements (see Hurtmans et al., 2012 and Ronsmans et al., 2016 for more details). In order to expand on the comparisons against FTIR measurements which is impossible during the polar night, Figure 1 (top panel) presents the time series of daily IASI total HNO_3 columns co-located with MLS VMR measurements within 2.5×2.5 grid boxes at three pressure levels (at 30, 50 and 70 hPa), averaged in the 70° - 90° S equivalent latitude band. Similar variations in HNO_3 are captured by the two instruments with an excellent agreement for the timing of the strong HNO_3 depletion within the inner vortex core. IASI HNO_3 variations generally match well those of MLS HNO_3 in each latitude band (see Figure 1 bottom panel for the 50° - 70° S equivalent latitude band; the other bands are not shown here).

Quality flags similar to those developed for O_3 in previous IASI studies (Wespes et al., 2017) were applied a posteriori to exclude data (i) with a corresponding poor spectral fit (e.g. based on quality flags rejecting biased or sloped residuals, fits with maximum number of iteration exceeded), (ii) with less reliability (e.g. based on quality flags rejecting suspect averaging kernels, data with less sensitivity characterized by a DOFS lower than 0.9) or (iii) with tropospheric cloud contamination (defined by a fractional cloud cover ≥ 25 %). Note that the HNO_3 total column distributions illustrated in sections below use the median as a statistical average since it is more robust against the outliers than the mean.

Temperature and potential vorticity (PV) fields are taken from the ECMWF ERA Interim Reanalysis dataset, respectively at 50 hPa and at the potential temperature of 530 K (corresponding to ~20 km altitude where the IASI sensitivity to HNO_3 is the highest during the Southern Hemisphere (S.H.) winter (Ronsmans et al., 2016). Because the HNO_3 uptake by PSCs starts a few degrees or slightly below T_{NAT}

(~195.7 K at 50 hPa (Hanson and Mauersberger, 1988)) depending on the meteorological conditions (Pitts et al., 2013; Hoyle et al., 2013; Lambert et al., 2016; Pitts et al., 2018), a threshold temperature of 195 K is considered in the sections below to identify the PSCs-containing regions. The potential vorticity is used to delimit dynamically consistent areas in the polar regions. In what follows, we use either the equivalent latitudes ("eqlat", calculated from PV fields at 530 K) or the PV values to characterize the relationship between HNO_3 and temperatures in the cold polar regions. Uncertainties in ERA-Interim temperatures will also be discussed below.

3 Annual cycle of HNO_3 vs temperatures

Figure 2a shows the yearly HNO_3 cycle (solid lines, left axis) in the southernmost equivalent latitudes (70° - 90° S), as measured by IASI over the whole period of measurements (2008–2017). The total HNO_3 variability in such equivalent latitudes has already been discussed in a previous IASI study (Ronsmans et al., 2018) where the contribution of the PSCs into the HNO_3 variations was highlighted. The temperature time series, taken at 50 hPa, is here represented as well (dashed lines, right axis). From this figure, different regimes of HNO_3 total columns *vs* temperature can be observed throughout the year and from one year to another. In particular, we define here three main regimes (R1, R2 and R3) along the HNO_3/temperature cycle. The full cycle and the main regimes in the 70° - 90° S eqlat region are further represented in Fig. 2b that shows a histogram of the HNO_3 total columns as a function of temperature for the year 2011. Similar histograms are observed for the ten years of IASI measurements (not shown). The red horizontal and vertical lines in Fig. 2a and Fig. 2b, respectively, represent the 195 K threshold temperature used to identify the onset of HNO_3 uptake by PSCs (see Section 2). The three identified regimes correspond to:

- R1 is defined by the maxima in the total HNO_3 abundances covering the months of April and May (~3×10^{16} molec.cm^{-2}, R1 in Figures 2a and b), when the 50 hPa temperature strongly decreases (from ~220 to ~195 K). These high HNO_3 levels result from low sunlight, preventing photodissociation, along with the heterogeneous hydrolysis of N_2O_5 to HNO_3 during autumn before the formation of polar stratospheric clouds (Keys et al., 1993; Santee et al., 1999; Urban et al., 2009; de Zafra and Smyshlyaev, 2001). This period also corresponds to the onset of the deployment of the southern polar vortex which is characterized by strong diabatic descent with weak latitudinal mixing across its boundary, isolating polar HNO_3-rich air from lower latitudinal airmasses.

- R2 which extends from June to October is characterized by the onset of the strong decrease in HNO_3 total columns at the beginning of June, when the temperatures fall below 195 K, followed by a plateau of total HNO_3 minima. In this regime, the HNO_3 total columns average below 2×10^{16} molec.cm^{-2} and the 50 hPa temperatures range mostly between 180 and 190 K.

- R3 starts in October when sunlight returns and the 50 hPa temperatures rise above 195 K. Despite the stratospheric warming with 50 hPa temperatures up to 240 K in summer, the HNO_3 total columns stagnate at the R2 plateau levels (around 1.5×10^{16} molec.cm^{-2}). This regime likely reflects the photolysis of NO_3 and HNO_3 itself (Ronsmans et al., 2018) as well as the permanent denitrification of the mid-stratosphere, caused by the PSCs sedimentation. The likely renitrification of the lowermost stratosphere (Braun et al., 2019; Lambert et al., 2012) where the HNO_3 concentrations and the IASI sensitivity to HNO_3 are lower (Ronsmans et al., 2016) cannot be inferred from the IASI measurements.The plateau lasts until approximately February, where HNO_3 total column slowly starts increasing, reaching the April-May maximum in R1.

As illustrated in Fig. 2a, the three regimes are observed each year with, however, some interannual variations. For instance, the sudden stratospheric warming (SSW) that occurs in 2010 (see the temperature time series at 20 hPa for the year 2010; green dotted line) yielded higher HNO_3 total columns (see green solid line in July and August) (de Laat and van Weele, 2011; Klekociuk et al., 2011; WMO, 2014; Ronsmans et al., 2018).

Figure 2c shows the evolution of the relationship between the daily averaged HNO_3 (calculated from a 7-day moving average) with the highest occurrence (in bins of 0.1×10^{16} molec.cm^{-2} and of 2K) and the 50 hPa temperature, over the 10 years of IASI. The red vertical line represents the 195 K threshold temperature. Figure 2c clearly illustrates the slow increase in HNO_3 columns as the temperatures decrease (February to May, i.e. R3 to R1), the strong and rapid HNO_3 depletion occurring in June (R2), the plateau of low HNO_3 abundances in winter and spring (from August to November; R2 to R3). Figure 2c also highlights the interannual variability in total HNO_3, which is found to be the largest in R3, and shows a strong consistency in the onset of the depletion between each year (beginning of June when the temperatures fall below 195 K as indicated by the red vertical line). Given the span of PSCs formation over a large range of altitudes (typically between 10 and 30 km) (Höpfner et al., 150 2006, 2009; Spang et al., 2018; Pitts et al., 2018) and that of maximum IASI sensitivity to HNO_3 around 50 hPa (Hurtmans et al., 2012; Ronsmans et al., 2016), the temperatures at two other pressure levels, namely 70 and 30 hPa (i.e. ~15 and ~25 km), have also been tested to investigate the relationship between HNO_3 and temperature in the low and mid-stratosphere. The results (not shown here) exhibit a similar HNO_3-temperature behavior at the different levels with, as expected, lower and larger temperatures in R2, respectively, at 30 hPa (down to ~180 K) and at 70 hPa (down to ~185 K), but still below the NAT formation threshold at these pressure levels (T_{NAT} ~193 K at 30 hPa and ~197 K at 70 hPa) (Lambert et al., 2016). Therefore, the altitude range of maximum IASI sensitivity to HNO_3 (see Section 2) is characterized by temperatures that are below the NAT formation threshold at these pressure levels, enabling the PSCs formation and the denitrification process. Furthermore, the consistency between the 195 K threshold temperature taken at 50 hPa and the onset of the strong total HNO_3 depletion seen in IASI data (see Fig. 2a and Fig. 2c) is in agreement with the largest NAT area that starts to develop in June around 20 km (Spang et al., 2018), which justifies the use of the 195 K temperature at that single representative level in this study.

4 Onset of HNO_3 depletion and drop temperature detection

To identify the spatial and temporal variability of the onset of the depletion phase, the daily time evolution of HNO_3 during the first 10 years of IASI measurements and the temperatures at 50 hPa are explored. In particular, the second derivative of HNO_3 total column with respect to time is calculated to detect the strongest rate of decrease seen in the HNO_3 time series and to identify its associated day and 50 hPa temperature.

4.1 HNO_3 vs temperature time series

Figure 3 shows the time series of the second derivative of HNO_3 total column with respect to time (blue) and of the temperature (red) averaged in the areas of potential vorticity smaller than -10×10^{-5} K.m^2.kg^{-1}.s^{-1} to encompass the regions inside the inner polar vortex where the temperatures are the coldest and the total HNO_3 depletion occurs (Ronsmans et al., 2018). The use of that PV threshold value explains the gaps in the time series during the summer when the PV does not reach such low levels, while the time series averaged in the 70°- 90° S Eqlat band (dashed blue for the second derivative of HNO_3 and grey for the temperature) covers the full year. Note that the HNO_3 time series has been smoothed with a simple spline data interpolation function to avoid gaps in order to calculate the second derivative of

HNO_3 total column with respect to time as the daily second-difference HNO_3 total column. The horizontal red line shows the 195 K threshold.

As already illustrated in Fig. 2a and Fig. 2c, the strongest rate of HNO_3 depletion (i.e. the second derivative minimum) is found around the 195 K threshold temperature, within some days (4 to 23 days) after total HNO_3 reaches its maximum, i.e. typically between the 11th of May (2013) and the 8th of June (2009). The 50 hPa drop temperatures are detected between 189.2 K and 202.8 K, with an average of 194.2 ± 3.8 K (1σ standard deviation) over the ten years. Knowing that T_{NAT} can be higher or lower depending on the atmospheric conditions and that NAT starts to nucleate from_2–4 K below T_{NAT} (Pitts et al., 2011; Hoyle et al., 2013; Lambert et al., 2016), the results here demonstrate the consistency between the 50 hPa drop temperature, i.e. the temperature associated with the strongest HNO_3 depletion detected from IASI, and the NAT formation temperature in the mid-stratosphere at polar latitudes. It further justifies the use of the single 50 hPa level for characterizing and investigating the onset of HNO_3 depletion from IASI. Nevertheless, given the range of maximum IASI sensitivity to HNO_3 around 50 hPa, typically between 70 and 30 hPa (Ronsmans et al., 2016), the drop temperatures are also calculated at these two other pressure levels (not shown here) to estimate the uncertainty of the calculated drop temperature defined in this study at 50 hPa. The 30 hPa and 70 hPa drop temperatures range respectively over 185.7 K –194.9 K and over 194.8 K – 203.7 K, with an average of 192.0 ± 2.9 K and 198.0 ± 3.2 K (1σ standard deviation) over the ten years of IASI. The average values at 30 hPa and 70 hPa fall within the 1σ standard deviation associated with the average drop temperature at 50 hPa. It is also worth noting the agreement between the drop temperatures and the NAT formation threshold at these two pressure levels (T_{NAT} ~ 193 K at 30 hPa and ~197 K at 70 hPa) (Lambert et al., 2016).

Figures 4a and b show the zonal distribution of HNO_3 total columns and of the temperature at 50 hPa, respectively, spanning 55° - 90° S over the whole IASI period, with, superimposed, three isocontour levels of potential vorticity (-10, -8 and -5×10^{-5} $K.m^2.kg^{-1}.s^{-1}$ in blue, cyan and black, respectively) and one isocontour for the 50 hPa temperature. The PV isocontour of -10×10^{-5} $K.m^2.kg^{-1}.s^{-1}$ is clearly shown to separate well the region of strong depletion in total HNO_3 according to the latitude and the time. The red vertical dashed lines indicates the average date for the drop temperatures calculated in the area of PV≤ -10×10^{-5} $K.m^2.kg^{-1}.s^{-1}$ (194.2 ± 3.8 K; see Fig. 3) over the IASI period. It shows that the strongest rate in HNO_3 depletion occurs on average a few days before June. The delay of some days between the maximum in total HNO_3 and the start of the depletion (see Fig. 3) is also visible in Fig. 4a. The yearly zonally averaged time series over the ten years of IASI can be found in Fig. 5; it shows the reproducibility of the edge of the collar HNO_3 region and of the region of the strong HNO_3 depletion, respectively delimited by the PV isocontours of -5×10^{-5} $K.m^2.kg^{-1}.s^{-1}$ and of -10×10^{-5} $K.m^2.kg^{-1}.s^{-1}$ at 50 hPa, measured by IASI from year to year.

4.2 Distribution of drop temperatures

To explore the capability of IASI to monitor the onset of HNO_3 depletion at a large scale from year to year, figure 6 shows the spatial distribution of the 50 hPa drop temperatures (based on the second derivative minima of total HNO_3 averaged in 1°×1° grid cells) inside a region delimited by a PV value of -8×10^{-5} $K.m^2.kg^{-1}.s^{-1}$, for each year of the IASI period. The green~~red~~ contour represents the PV isocontour of -10×10^{-5} $K.m^2.kg^{-1}.s^{-1}$, averaged over the period 10 May – 15 July for each year, which delimits our region of interest. The isocontours of 195 K for the average temperatures and the minimum temperatures, as well as the isocontour of -10×10^{-5} $K.m^2.kg^{-1}.s^{-1}$ for the minimum PV encountered at 50 hPa over the 10 May to 15 July period are also represented. The calculated drop temperatures corresponding to the onset of HNO_3 depletion inside the averaged PV isocontour are found to vary between ~180 and ~210 K and the corresponding dates range between ~mid-May and mid-July (not shown here). Note that the high extremes in the drop temperature, which are found in some cases above eastern Antarctica, should be considered with caution: they correspond to specific regions above ice surface with emissivity features that are known to yield errors in the IASI retrievals (Hurtmans et al., 2012; Ronsmans et al., 2016). Indeed, bright land surface such as ice might in some cases lead to poor HNO_3 retrievals. Although wavenumber-dependent surface emissivity atlases are used in FORLI (Hurtmans et al., 2012), this parameter remains critical and causes poorer retrievals that, in some instances, pass through the series of quality filters and could affect the drop temperature calculation.

The averaged isocontour of 195 K encircles well the area of HNO_3 drop temperatures lower than 195 K (typically from ~187 K to ~195 K), which means that the bins inside that area characterize airmasses that experience the NAT threshold temperature during a long time over the 10 May – 15 July period. That area encompasses the inner vortex core (delimited by the isocontour of -10×10^{-5} $K.m^2.kg^{-1}.s^{-1}$ for the PV averaged over the 10 May – 15 July period) and show pronounced minima (lower than -0.5×10^{14} $molec.cm^{-2}.d^{-2}$) in the second derivative of the HNO_3 total column with respect to time (not shown here), which indicate a strong and rapid HNO_3 depletion. The area enclosed between the two isocontours of 195 K for the temperatures, the averaged one and the one for the minimum temperatures, show generally higher drop temperatures and weakest minima (larger than -0.5×10^{14} $molec.cm^{-2}.d^{-2}$) in the second derivative of the HNO_3 total column (not shown). That area is also enclosed by the isocontour of -10×10^{-5} $K.m^2.kg^{-1}.s^{-1}$ for the minimum PV, meaning that the bins inside correspond, at least for one day over the 10 May – 15 July period, to airmasses located at the inner edge of the vortex and characterized by temperature lower than the NAT threshold temperature. The weakest minima in the second derivative of total HNO_3 (not shown) observed in that area indicate a weak and slow HNO_3 depletion and might be explained by a short period of the NAT threshold temperature experienced at the inner edge of the vortex. It could also reflect a mixing with strong HNO_3-depleted and colder airmasses from the inner vortex core. The mixing with these already depleted airmasses could also explained the higher drop temperatures detected in those bins. These high drop temperatures are generally detected later (after the HNO_3 depletion occurs, i.e. after the 10 May – 15 July period considered here – not shown), which supports the transport, in those bins, of earlier HNO_3-depleted airmasses and the likely mixing at the edge of the vortex. Finally, these spatial variations might also partly reflect the range of maximum sensitivity of IASI to HNO_3, while biases in ECMWF reanalysis are too small for explaining the spatial variation in drop temperatures. Thanks to the assimilation of an advanced Tiros Operational Vertical Sounder (ATOVS) around 1998–2000 in reanalyses, to the better coverage of satellite instruments and to the use of global navigation satellite system (GNSS) radio occultation (RO) (Schreiner et al., 2007; Wang et al., 2007; Lambert and Santee, 2018; Lawrence et al., 2018), the uncertainties have been vastly reduced. Comparisons of the ECMWF ERA Interim dataset used in this work with the COSMIC data (Lambert and Santee, 2018) found a small warm bias, with median differences around 0.5 K, reaching 0–0.25 K in the southernmost regions of the globe at ~68–21 hPa where PSCs form.

Except above some parts of Antarctica which are prone to larger retrieval errors, the overall range in the drop 50 hPa temperature for total HNO_3 inside the isocontour for the averaged temperature of 195 K, typically extends from ~187 K to ~195 K, which falls within the range of PSCs nucleation temperature at 50 hPa: from slightly below T_{NAT} to around 3-4 K below the ice frost point - T_{ice} - depending on atmospheric conditions, on TTE and on the type of formation mechanisms (Pitts et al., 2011; Peter and Grooß, 2012; Hoyle et al., 2013). This underlines well the benefit of the excellent spatial and temporal coverage of IASI that allows to capture the rapid and critical depletion phase over a large scale.

5 Conclusions

In this paper, we have explored the added value of the dense HNO_3 total columns dataset provided by the IASI/Metop satellite over a full decade (2008–2017) for monitoring the stratospheric depletion phase that occurs each year in the S.H. and for investigating its relationship to the NAT formation temperature. To that end, we focused on and delimited the coldest polar region of the S.H. using a specific PV value at 530 K (~50 hPa, PV of -10×10^{-5} K.m^2.kg^{-1}.s^{-1}) and stratospheric temperatures at 50 hPa, taken from the ECMWF ERA Interim reanalysis. That single representative pressure level has been considered in this study given the maximum sensitivity of IASI to HNO_3 around that level over a range where the PSCs formation/denitrification process occur.

The annual cycle of total HNO_3, as observed from IASI, has first been characterized according to the temperature evolution. Three various regimes (R1 to R3) in the total HNO_3 - 50 hPa temperature relationship were highlighted from the time series over the S.H. polar region and described along the cycle: R1 is defined at play during April and May and characterized by a rapid decrease in 50 hPa temperatures while HNO_3 accumulates in the poles; R2, from June to September, shows the onset of the depletion when the 50 hPa temperatures fall below 195 K (considered here as the onset of PSCs nucleation phase at that level), with a strong consistency between each year; R3, defined from November until March when total HNO_3 remains at low R2 plateau levels, despite the return of sunlight and heat, characterizes the strong denitrification of the stratosphere, likely due to PSCs sedimentation at lower levels where the IASI sensitivity is low. For each year over the IASI period, the use of the second derivative of the HNO_3 column versus time was then found particularly valuable to detect the onset of the HNO_3 condensation to PSCs. It is captured, on average from IASI, a few days before June with a delay of 4–23 days after the maximum in total HNO_3. The corresponding temperatures ('drop temperatures') were detected between 189.2 K and 202.8 K (194.2 ± 3.8 on average over the 10 years), which demonstrated the good consistency between the 50 hPa drop temperature and the PSCs formation temperatures in that altitude region. Finally, the annual and spatial variability (within 1°× 1°) in the drop temperature was further explored from IASI total HNO_3. Inside the isocontours of 195 K for the average temperatures and of -10×10^{-5} K.m^2.kg^{-1}.s^{-1} for the averaged PV at 50 hPa, the drop temperatures are detected between ~mid-May and mid-July, typically range between ~187 K to ~195 K and are associated with the highest minima (lower than -0.5×10^{14} molec.cm^{-2}.d^{-2}) in the second derivative of the HNO_3 total column with respect to time, indicating a strong and rapid HNO_3 depletion. Except for extreme drop temperatures (~210 K) that were found from year to year above eastern Antarctica and suspected to result from unfiltered poor quality retrievals in case of emissivity issues above ice, the range of drop temperatures is interestingly found in line with the PSCs nucleation temperature that is known, from previous studies, to strongly depend on a series a factors (e.g. meteorological conditions, HNO_3 vapour pressure, temperature threshold exposure, presence of meteoritic dust). At the edge of the vortex, considering the isocontours of 195 K for the minimum temperatures or of -10×10^{-5} K.m^2.kg^{-1}.s^{-1} for the minimum PV, higher and later drop temperatures along with weakest minima in the second derivative of the HNO_3 total column with respect to time, indicating a slow HNO_3 depletion, are found. It likely results from a short temperature threshold exposure or a mixing with already depleted airmasses from the inner vortex core. The results of this study highlight the ability of IASI to measure the variations in total HNO_3 and, in particular, to capture and monitor the rapid depletion phase over the whole polar regions.

We show in this study that the IASI dataset allows capturing the variability of stratospheric HNO_3 throughout the year (including the polar night) in the Antarctic. In that respect, it offers a new observational means to monitor the relation of HNO_3 to temperature and the related formation of PSCs. Despite the limited vertical resolution of IASI which does not allow to investigate the HNO_3 uptake by the different types of PSCs during their formation and growth along the vertical profile, the HNO_3 total column measurements from IASI constitute an important new dataset for exploring the strong polar depletion over the whole stratosphere. This is particularly relevant considering the mission continuity, which will span several decades with the planned follow-on missions. Indeed, thanks to the three successive instruments (IASI-A launched in 2006 and still operating, IASI-B in 2012, and IASI-C in 2018) that demonstrate an excellent stability of the Level-1 radiances, the measurements will soon provide an unprecedented long-term dataset of HNO_3 total columns. Further work could also make use of this unique data set to investigate the relation between HNO_3, O_3, and meteorology in the changing climate.

Data availability

The IASI HNO_3 data processed with FORLI-HNO_3 v0151001 are available upon request to the corresponding author.

Author contributions

G.R. performed the analysis, wrote the manuscript and prepared the figures. C.W. and L.C. contributed to the analysis. C.W., S.S., P.-F. C. and L.C. contributed to the interpretation of the results. D.H. was responsible for the retrieval algorithm development and the processing of the IASI HNO_3 dataset. All authors contributed to the writing of the text and reviewed the manuscript.

Competing interests

The authors declare no competing interests.

Acknowledgements

IASI has been developed and built under the responsibility of the Centre National d’Etudes Spatiales (CNES, France). It is flown on board the Metop satellites as part of the EUMETSAT Polar System. The IASI L1 data are received through the EUMETCast near-real-time data distribution service. The research was funded by the F.R.S.-FNRS, the Belgian State Federal Office for Scientific, Technical and Cultural Affairs (Prodex arrangement 4000111403 IASI.FLOW) and EUMETSAT through the Satellite Application Facility on Atmospheric Composition Monitoring (ACSAF). G. Ronsmans is grateful to the Fonds pour la Formation à la Recherche dans l’Industrie et dans l’Agriculture of Belgium for a PhD grant (Boursier FRIA). L. Clarisse is a research associate supported by the F.R.S.-FNRS. C. Clerbaux is grateful to CNES for financial support. S. Solomon is supported by the National Science Foundation (NSF-1539972).

Figure captions

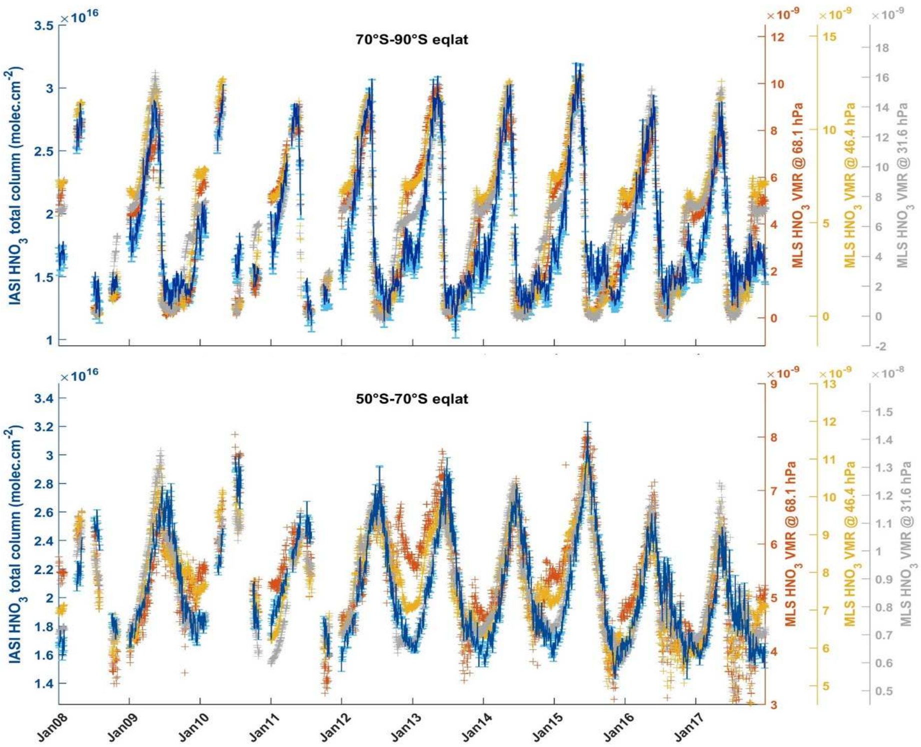

Figure 1. Time series of daily IASI total HNO_3 column (blue, left y-axis) co-located with MLS and of MLS VMR HNO_3 within 2.5×2.5 grid boxes at three pressure levels (at 30, 50 and 70 hPa; right y-axis), averaged in the 70°S–90°S (top panel) and in the 50°S–70°S (bottom panel) equivalent latitude bands. The error bars (light blue) represents 3σ, where σ is the standard deviation around the IASI HNO_3 daily average.

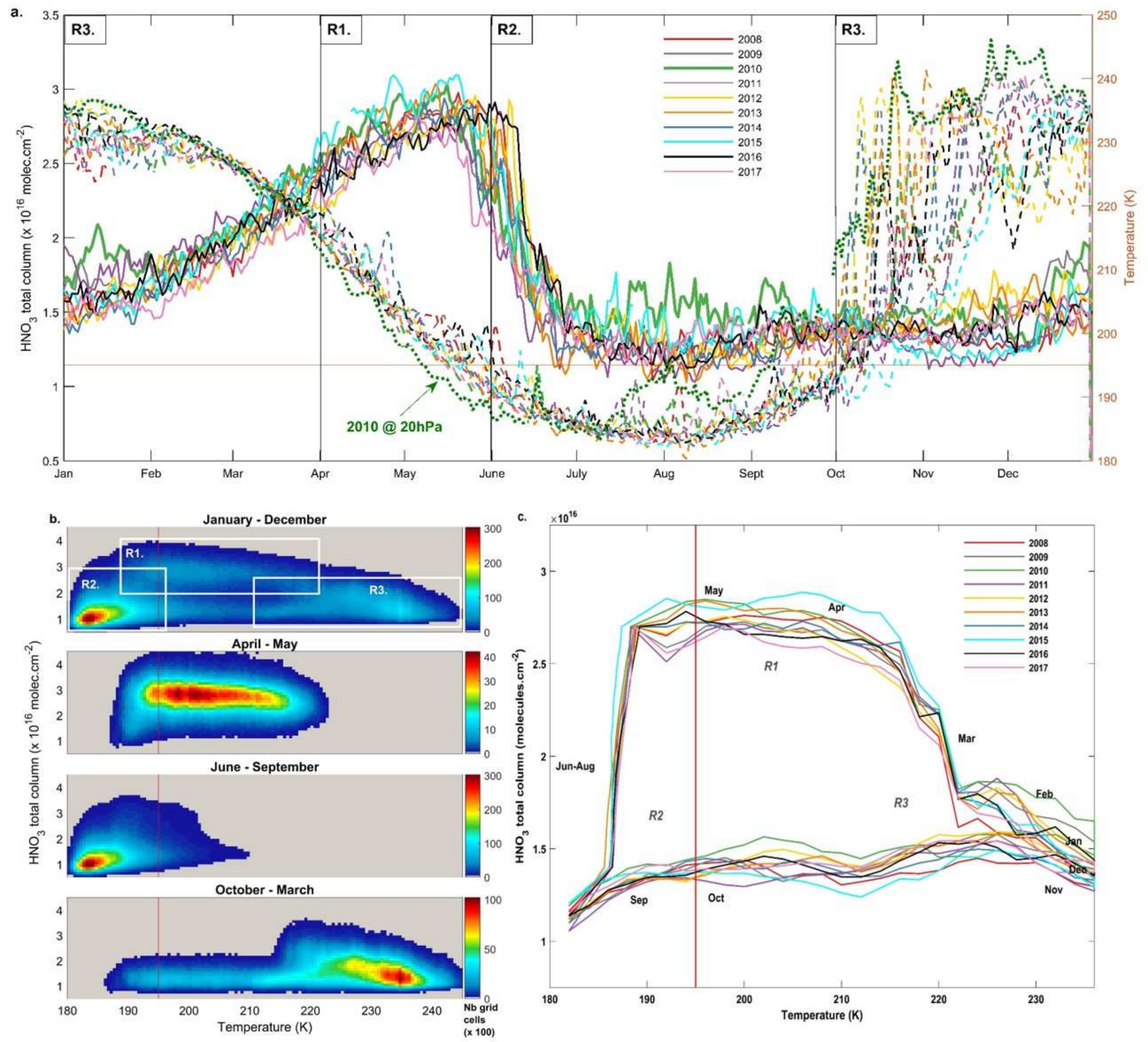

Figure 2. (a) Time series of daily averaged HNO_3 total columns (solid lines) and temperatures taken at 50 hPa (dashed lines) in the 70° - 90° S equivalent latitude band, for the years 2008 – 2017. The green dotted line represents the temperatures at 20 hPa for the year 2010. (b) HNO_3 total columns versus temperatures (at 50 hPa) histogram for the whole year (top) and for the 3 defined regimes (R1 - R3) separated in (a) for the year 2011. The colors refer to the number of gridded measurements in each cell. (c) Evolution of daily averaged HNO_3 total columns with the highest occurrence (in bins of 0.1×10^{16} molec.cm^{-2} and 2 K) as a function of the 50 hPa temperature for the years 2008 – 2017. The red horizontal or vertical lines represent the 195 K threshold temperature.

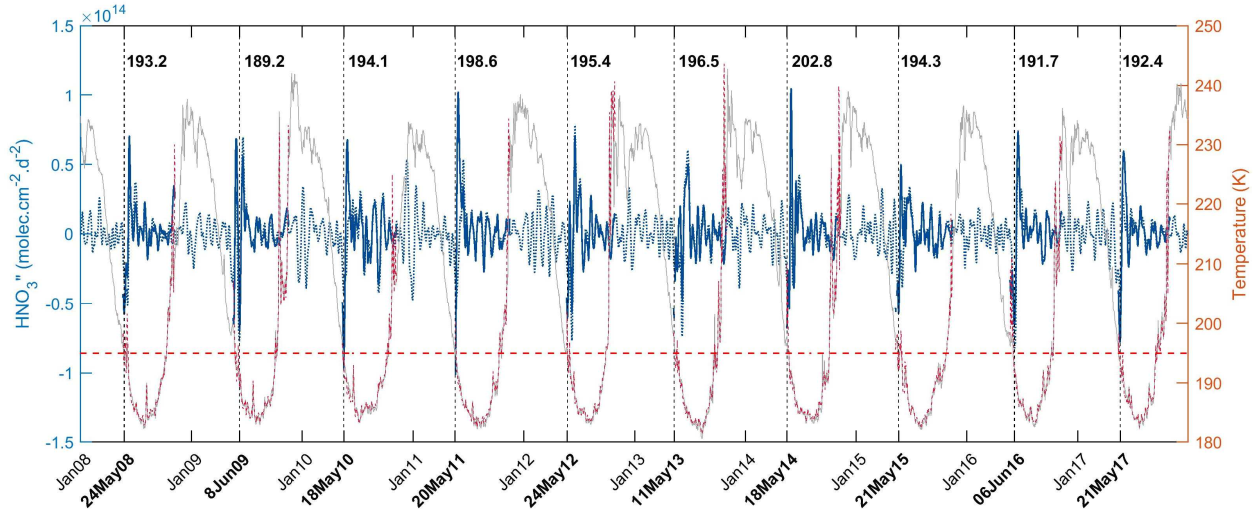

Figure 3. Time series of total HNO_3 second derivative (blue, left y-axis) and of the temperature (red, right y-axis), in the region of potential vorticity at 530 K lower than -10×10^{-5} K.m^2.kg^{-1}.s^{-1}. The red horizontal line corresponds to the 195 K temperature. The vertical dashed lines indicate the second derivative minimum in HNO_3 for each year. The corresponding dates (in bold, on the x-axis) and temperatures are also indicated. The time series of total HNO_3 second derivative (dashed blue) and of temperature (grey) in the 70° – 90° S Eqlat band are also represented.

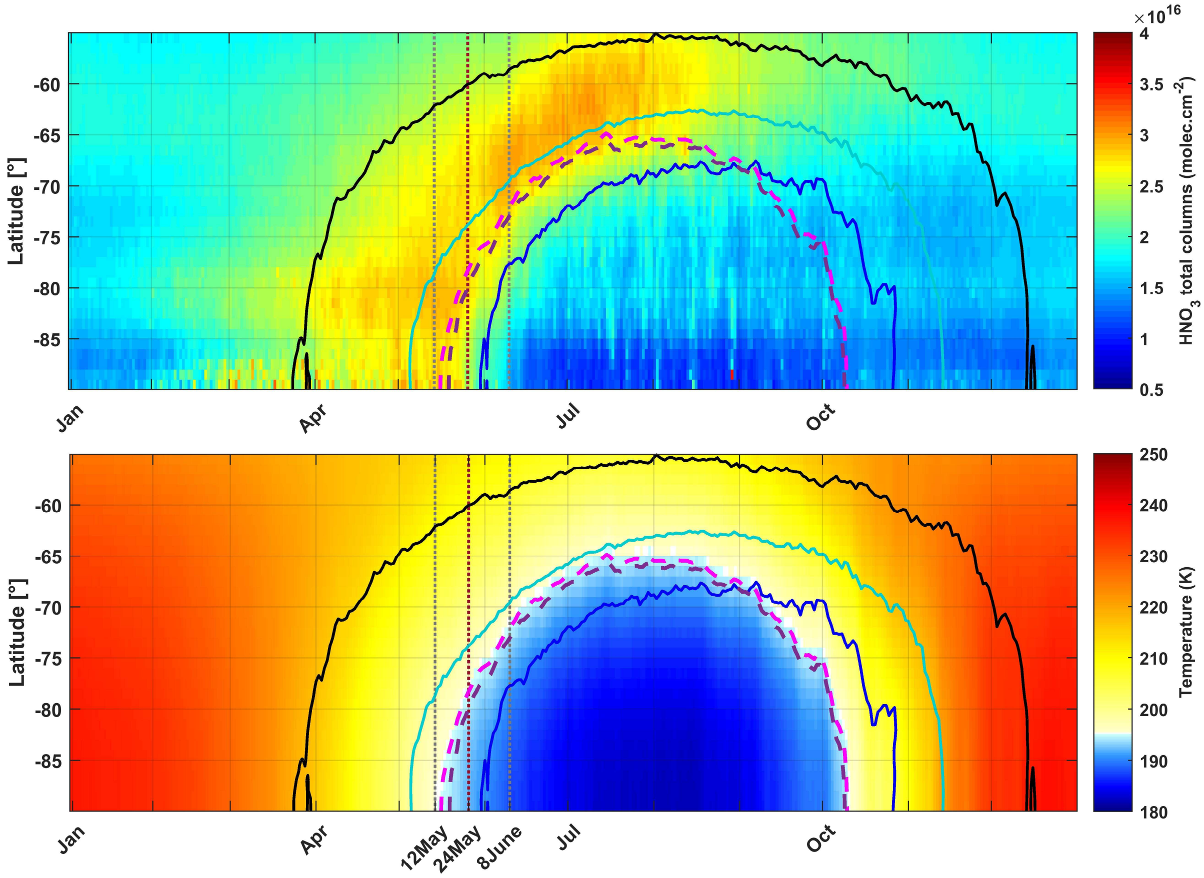

Figure 4. Zonal distributions of (a) HNO_3 total columns (in molec.cm^{-2}) from IASI and (b) temperatures at 50 hPa from ERA Interim (in K) between 55° to 90° south and averaged over the years 2008 – 2017. Three isocontours for PV of -5 (black), -8 (cyan) and -10 (blue) ($\times 10^{-5}$ K.m^2.kg^{-1}.s^{-1}) at 530 K, the isocontours for the 195 K temperature (pink) and for the averaged 194.2 K drop temperature (purple) at 50 hPa are superimposed. The vertical grey dashed lines encompass the period of the second derivative minima and the red one indicates the average date for the drop temperatures calculated in the area delimited by a -10×10^{-5} K.m^2.kg^{-1}.s^{-1} PV contour.

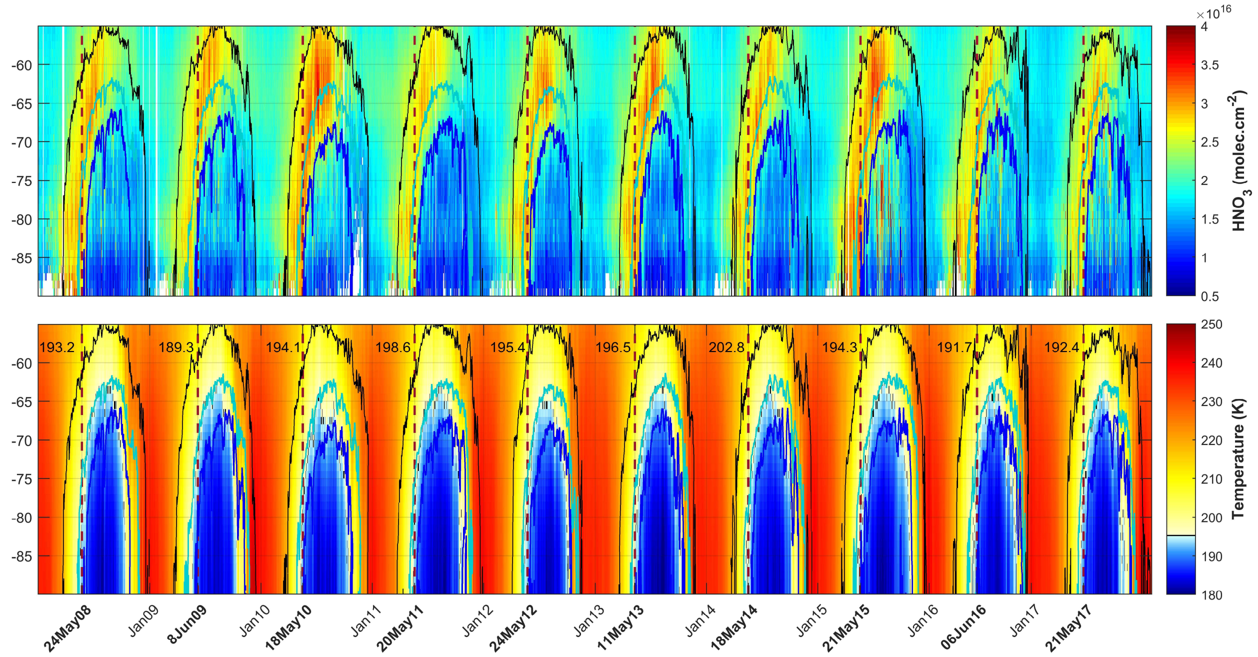

Figure 5. Zonally averaged distributions of (top) HNO_3 total columns (in molec.cm^{-2}) from IASI and (bottom) temperatures at 50 hPa from ERA Interim (in K). The latitude range is from 55° to 90° south and the isocontours are PVs of -5 (black), -8 (cyan) and -10 (blue) (× 10^{-5} K.m^2.kg^{-1}.s^{-1} at 530 K). The vertical red dashed lines correspond to the second derivative minima each year in the area delimited by a -10×10^{-5} K.m^2.kg^{-1}.s^{-1} PV contour.

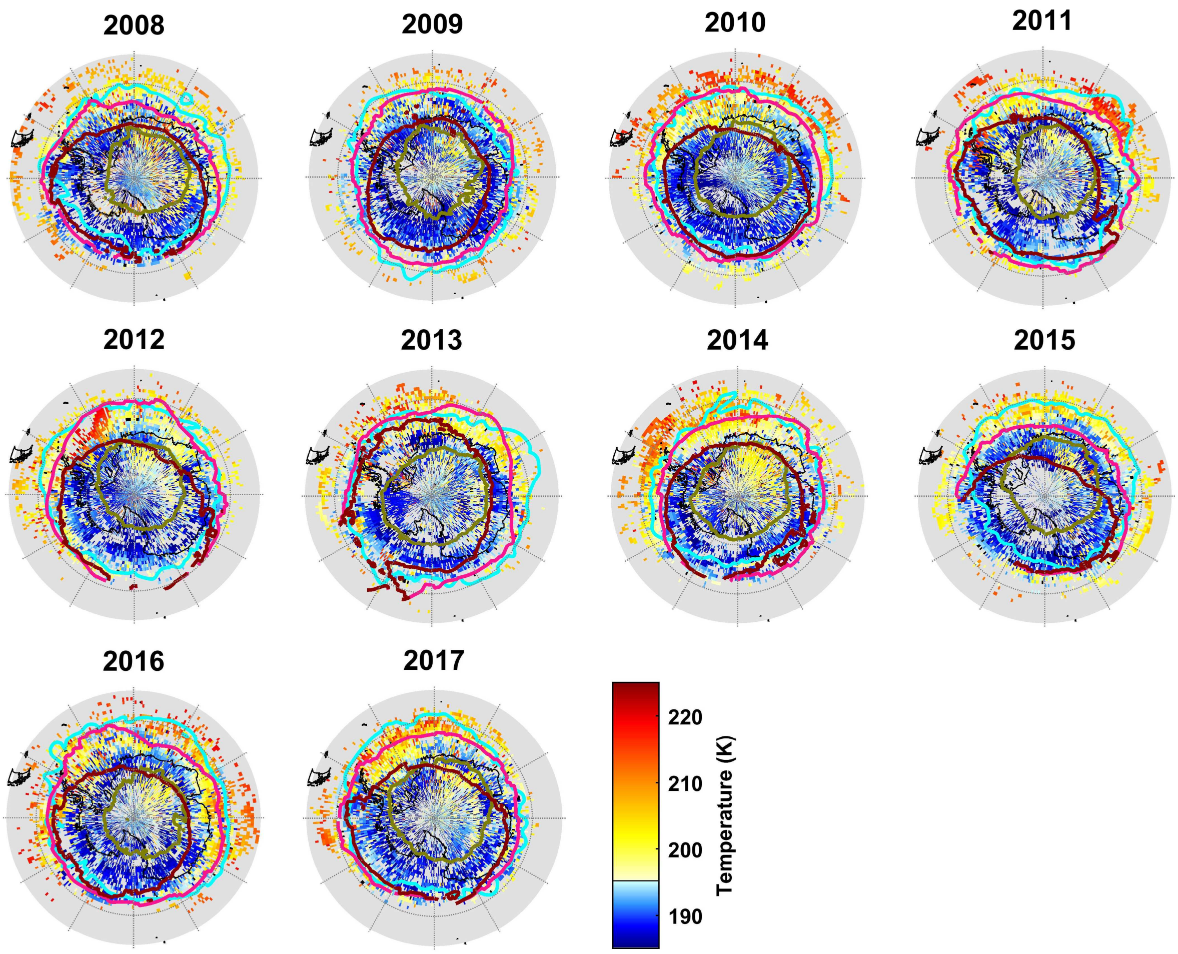

Figure 6. Spatial distribution (1°×1°) of the drop temperature at 50 hPa (K) (calculated from the total HNO_3 second derivative minima) for each year of IASI (2008–2017), in a region defined by a PV of -8×10^{-5} $K.m^2.kg^{-1}.s^{-1}$. The isocontours of -10×10^{-5} $K.m^2.kg^{-1}.s^{-1}$ at 530 K for the averaged PV (in green) and the minimum PV (in cyan) encountered over the period 10 May –15 June for each year and the isocontours of 195 K at 50 hPa for the averaged (in red) and the minimum (in pink) temperatures over the same period are represented.

References

Braun, M., Grooß, J.-U., Woiwode, W., Johansson, S., Höpfner, M., Friedl-Vallon, F., Oelhaf, H., Preusse, P., Ungermann, J., Sinnhuber, B.-M., Ziereis, H., and Braesicke, P.: Nitrification of the lowermost stratosphere during the exceptionally cold Arctic winter 2015/16, Atmospheric Chemistry and Physics Discussions, https://doi.org/10.5194/acp-2019-108, 2019.

Carslaw, K. S., Luo, B. P., and Peter, T.: An analytical expression for the composition of aqueous {HNO_3-H_2SO_4-H_2O} stratospheric aerosols including gas phase removal of HNO_3, Geophys. Res. Lett., 22, 1877–1880, https://doi.org/10.1029/95GL01668, 1995.

Carslaw, K. S., Wirth, M., Tsias, A., Luo, B. P., Dörnbrack, A., Leutbecher, M., Volkert, H., Renger, W., Bacmeister, J. T., Reimer, E., and Peter, T.: Increased stratospheric ozone depletion due to mountain-induced atmospheric waves, Nature, 391, 675–678, https://doi.org/10.1038/35589, 1998.

Clerbaux, C., Boynard, A., Clarisse, L., George, M., Hadji-Lazaro, J., Herbin, H., Hurtmans, D., Pommier, M., Razavi, A., Turquety, S., Wespes, C., and Coheur, P.-F.: Monitoring of atmospheric composition using the thermal infrared IASI/MetOp sounder, Atmospheric Chemistry and Physics, 9, 6041–6054, https://doi.org/10.5194/acp-9-6041-2009, 2009.

de Laat, A. T. J. and van Weele, M.: The 2010 Antarctic ozone hole: Observed reduction in ozone destruction by minor sudden stratospheric warmings, Scientific Reports, 1, 38, https://doi.org/10.1038/srep00038, 2011.

de Zafra, R. and Smyshlyaev, S. P.: On the formation of HNO3 in the Antarctic mid to upper stratosphere in winter, Journal of Geophysical Research, 106, 23 115, https://doi.org/10.1029/2000JD000314, 2001.

Grooß, J. U., Engel, I., Borrmann, S., Frey, W., Günther, G., Hoyle, C. R., Kivi, R., Luo, B. P., Molleker, S., Peter, T., Pitts, M. C., Schlager, H., Stiller, G., Vömel, H., Walker, K. a., and Müller, R.: Nitric acid trihydrate nucleation and denitrification in the Arctic stratosphere, Atmospheric Chemistry and Physics, 14, 1055–1073, https://doi.org/10.5194/acp-14-1055-2014, 2014.

Hanson, D. and Mauersberger, K.: Laboratory studies of the nitric acid trihydrate: Implications for the south polar stratosphere, Geophysical Research Letters, 15, 855–858, https://doi.org/10.1029/GL015i008p00855, 1988.

Harris, N. R. P., Lehmann, R., Rex, M., and von der Gathen, P.: A closer look at Arctic ozone loss and polar stratospheric clouds, Atmospheric Chemistry and Physics, 10, 8499–8510, https://doi.org/10.5194/acp-10-8499-2010, 2010.

Hilton, F., Armante, R., August, T., Barnet, C., Bouchard, A., Camy-Peyret, C., Capelle, V., Clarisse, L., Clerbaux, C., Coheur, P.-F., Collard, A., Crevoisier, C., Dufour, G., Edwards, D., Faijan, F., Fourrié, N., Gambacorta, A., Goldberg, M., Guidard, V., Hurtmans, D., Illingworth, S., Jacquinet-Husson, N., Kerzenmacher, T., Klaes, D., Lavanant, L., Masiello, G., Matricardi, M., McNally, A., Newman, S., Pavelin, E., Payan, S., Péquignot, E., Peyridieu, S., Phulpin, T., Remedios, J., Schlüssel, P., Serio, C., Strow, L., Stubenrauch, C., Taylor, J., Tobin, D., Wolf, W., and Zhou, D.: Hyperspectral Earth Observation from IASI: Five Years of Accomplishments, Bulletin of the American Meteorological Society, 93, 347–370, https://doi.org/10.1175/BAMS-D-11-00027.1, 2012.

Hoffmann, L., Spang, R., Orr, A., Alexander, M. J., Holt, L. A., and Stein, O.: A decadal satellite record of gravity wave activity in the lower stratosphere to study polar stratospheric cloud formation, Atmospheric Chemistry and Physics, 17, 2901–2920, https://doi.org/10.5194/acp-17-2901-2017, 2017.

Höpfner, M., Luo, B. P., Massoli, P., Cairo, F., Spang, R., Snels, M., Di Donfrancesco, G., Stiller, G., von Clarmann, T., Fischer, H., and Biermann, U.: Spectroscopic evidence for NAT, STS, and ice in MIPAS infrared limb emission measurements of polar stratospheric clouds, Atmospheric Chemistry and Physics, 6, 1201–1219, https://doi.org/10.5194/acp-6-1201-2006, 2006.

Höpfner, M., Pitts, M. C., and Poole, L. R.: Comparison between CALIPSO and MIPAS observations of polar stratospheric clouds, Journal of Geophysical Research Atmospheres, 114, 1–15, https://doi.org/10.1029/2009JDO12114, 2009.

Hoyle, C. R., Engel, I., Luo, B. P., Pitts, M. C., Poole, L. R., Grooß, J. U., and Peter, T.: Heterogeneous formation of polar stratospheric clouds- Part 1: Nucleation of nitric acid trihydrate (NAT), Atmospheric Chemistry and Physics, 13, 9577–9595, https://doi.org/10.5194/acp-13- 9577-2013, 2013.

Hurtmans, D., Coheur, P.-F., Wespes, C., Clarisse, L., Scharf, O., Clerbaux, C., Hadji-Lazaro, J., George, M., and Turquety, S.: FORLI radiative transfer and retrieval code for IASI, Journal of Quantitative Spectroscopy and Radiative Transfer, 113, 1391–1408, https://doi.org/10.1016/j.jqsrt.2012.02.036, 2012.

James, A. D., Brooke, J. S. A., Mangan, T. P., Whale, T. F., Plane, J. M. C., and Murray, B. J.: Nucleation of nitric acid hydrates in polar stratospheric clouds by meteoric material, Atmospheric Chemistry and Physics, 18, 4519–4531, https://doi.org/10.5194/acp-18-4519- 2018, 2018.

Keys, J. G., Johnston, P. V., Blatherwick, R. D., and Murcray, F. J.: Evidence for heterogeneous reactions in the Antarctic autumn stratosphere, Nature, 361, 49–51, https://doi.org/10.1038/361049a0, 1993.

Klekociuk, A., Tully, M., Alexander, S., Dargaville, R., Deschamps, L., Fraser, P., Gies, H., Henderson, S., Javorniczky, J., Krummel, P., Petelina, S., Shanklin, J., Siddaway, J., and Stone, K.: The Antarctic ozone hole during 2010, Australian Meteorological and Oceanographic Journal, 61, 253–267, https://doi.org/10.22499/2.6104.006, 2011.

Koop, T., Luo, B., Tsias, A., and Peter, T.: Water activity as the determinant for homogeneous ice nucleation in aqueous solutions, Nature, 406, 611–614, https://doi.org/10.1038/35020537, 2000.

Kvissel, O.-K., Orsolini, Y. J., Stordal, F., Isaksen, I. S. A., and Santee, M. L.: Formation of stratospheric nitric acid by a hydrated ion cluster reaction: Implications for the effect of energetic particle precipitation on the middle atmosphere, Journal of Geophysical Research: Atmospheres, 117, n/a–n/a, https://doi.org/10.1029/2011jd017257, 2012.

Lambert, A. and Santee, M. L.: Accuracy and precision of polar lower stratospheric temperatures from reanalyses evaluated from A-Train CALIOP andMLS, COSMIC GPS RO, and the equilibrium thermodynamics of supercooled ternary solutions and ice clouds, Atmospheric Chemistry and Physics, 18, 1945–1975, https://doi.org/10.5194/acp-18-1945-2018, 2018.

Lambert, A., Santee, M. L., Wu, D. L., and Chae, J. H.: A-train CALIOP and MLS observations of early winter Antarctic polar stratospheric clouds and nitric acid in 2008, Atmospheric Chemistry and Physics, 12, 2899–2931, https://doi.org/10.5194/acp-12-2899-2012, 2012.

Lambert, A., Santee, M. L., and Livesey, N. J.: Interannual variations of early winter Antarctic polar stratospheric cloud formation and nitric acid observed by CALIOP and MLS, Atmospheric Chemistry and Physics, 16, 15 219–15 246, https://doi.org/10.5194/acp-16-15219-2016, 2016.

Lawrence, Z. D., Manney, G. L., and Wargan, K.: Reanalysis intercomparisons of stratospheric polar processing diagnostics, Atmospheric Chemistry and Physics, 18, 13 547–13 579, https://doi.org/10.5194/acp-18-13547-2018, 2018.

Lowe, D. and MacKenzie, A. R.: Polar stratospheric cloud microphysics and chemistry, Journal of Atmospheric and Solar-Terrestrial Physics, 70, 13–40, https://doi.org/10.1016/j.jastp.2007.09.011, 2008.

Molleker, S., Borrmann, S., Schlager, H., Luo, B., Frey, W., Klingebiel, M., Weigel, R., Ebert, M., Mitev, V., Matthey, R., Woiwode, W., Oelhaf, H., Dörnbrack, A., Stratmann, G., Grooß, J.-U., Günther, G., Vogel, B., Müller, R., Krämer, M., Meyer, J., and Cairo, F.: Microphysical properties of synoptic-scale polar stratospheric clouds: in situ measurements of unexpectedly large HNO3-containing particles in the Arctic vortex, Atmospheric Chemistry and Physics, 14, 10 785–10 801, https://doi.org/10.5194/acp-14-10785-2014, 2014.

Murphy, D. M. and Koop, T.: Review of the vapour pressures of ice and supercooled water for atmospheric applications, Quarterly Journal of the Royal Meteorological Society, 131, 1539–1565, https://doi.org/10.1256/qj.04.94, 2005.

Peter, T.: Microphysics and heterogeneous chemistry of polar stratospheric clouds, Annual Review of Physical Chemistry, 48, 785–822, https://doi.org/10.1146/annurev.physchem.48.1.785, 1997.

Peter, T. and Grooß, J.-U.: Chapter 4. Polar Stratospheric Clouds and Sulfate Aerosol Particles: Microphysics, Denitrification and Heterogeneous Chemistry, in: Stratospheric Ozone Depletion and Climate Change, pp. 108–144, Royal Society of Chemistry, https://doi.org/10.1039/9781849733182-00108, 2012.

Piccolo, C. and Dudhia, A.: Precision validation of MIPAS-Envisat products, Atmospheric Chemistry and Physics, 7, 1915–1923, https://doi.org/10.5194/acp-7-1915-2007, 2007.

Pitts, M. C., Poole, L. R., Dörnbrack, A., and Thomason, L. W.: The 2009-2010 Arctic polar stratospheric cloud season: A CALIPSO perspective, Atmospheric Chemistry and Physics, 11, 2161–2177, https://doi.org/10.5194/acp-11-2161-2011, 2011.

Pitts, M. C., Poole, L. R., Lambert, A., and Thomason, L.W.: An assessment of CALIOP polar stratospheric cloud composition classification, Atmospheric Chemistry and Physics, 13, 2975–2988, https://doi.org/10.5194/acp-13-2975-2013, 2013.

Pitts, M. C., Poole, L. R., and Gonzalez, R.: Polar stratospheric cloud climatology based on CALIPSO spaceborne lidar measurements from 2006 to 2017, Atmospheric Chemistry and Physics, 18, 10 881–10 913, https://doi.org/10.5194/acp-18-10881-2018, 2018.

Rodgers, C. D.: Inverse Methods for Atmospheric Sounding - Theory and Practice, vol. 2 of Series on Atmospheric Oceanic and Planetary Physics, World Scientific Publishing Co. Pte. Ltd., https://doi.org/10.1142/9789812813718, 2000.

Ronsmans, G., Langerock, B., Wespes, C., Hannigan, J. W., Hase, F., Kerzenmacher, T., Mahieu, E., Schneider, M., Smale, D., Hurtmans, D., De Mazière, M., Clerbaux, C., and Coheur, P.-F.: First characterization and validation of FORLI-HNO3 vertical profiles retrieved from IASI/Metop, Atmospheric Measurement Techniques, 9, 4783–4801, https://doi.org/10.5194/amt-9-4783-2016, 2016.

Ronsmans, G.,Wespes, C., Hurtmans, D., Clerbaux, C., and Coheur, P.-F.: Spatio-temporal variations of nitric acid total columns from 9 years of IASI measurements – a driver study, Atmospheric Chemistry and Physics, 18, 4403–4423, https://doi.org/10.5194/acp-18-4403-2018, 2018.

Santee, M. L., Manney, G. L., Froidevaux, L., Read, W. G., and Waters, J. W.: Six years of UARS Microwave Limb Sounder HNO_3 observations : Seasonal, interhemispheric, and interannual variations in the lower stratosphere, Journal of Geophysical Research, 104, 8225–8246, https://doi.org/10.1029/1998JD100089, 1999.

Santee, M. L., Lambert, A., Read, W. G., Livesey, N. J., Cofield, R. E., Cuddy, D. T., Daffer, W. H., Drouin, B. J., Froidevaux, L., Fuller, R. A., Jarnot, R. F., Knosp, B. W., Manney, G. L., Perun, V. S., Snyder, W. V., Stek, P. C., Thurstans, R. P., Wagner, P. A., Waters, J. W., Muscari, G., de Zafra, R. L., Dibb, J. E., Fahey, D. W., Popp, P. J., Marcy, T. P., Jucks, K. W., Toon, G. C., Stachnik, R. A., Bernath, P. F., Boone, C. D., Walker, K. A., Urban, J., and Murtagh, D.: Validation of the Aura Microwave Limb Sounder HNO3 measurements, Journal of Geophysical Research, 112, 1–22, https://doi.org/10.1029/2007JD008721, 2007.

Schreiner, J., Voigt, C., Weisser, C., Kohlmann, A., Mauersberger, K., Deshler, T., Kröger, C., Rosen, J., Kjome, N., Larsen, N., Adriani, A., Cairo, F., Donfrancesco, G. D., Ovarlez, J., Ovarlez, H., and Dörnbrack, A.: Chemical , microphysical , and optical properties of polar stratospheric clouds, Journal of Geophysical Research, 108, 1–10, https://doi.org/10.1029/2001JD000825, 2003.

Schreiner, W., Rocken, C., Sokolovskiy, S., Syndergaard, S., and Hunt, D.: Estimates of the precision of GPS radio occultations from the COSMIC/FORMOSAT-3 mission, Geophysical Research Letters, 34, 1–5, https://doi.org/10.1029/2006GL027557, 2007.

Sheese, P. E., Walker, K. A., Boone, C. D., Bernath, P. F., Froidevaux, L., Funke, B., Raspollini, P., and von Clarmann, T.: ACE-FTS ozone, water vapour, nitrous oxide, nitric acid, and carbon monoxide profile comparisons with MIPAS and MLS, Journal of Quantitative Spectroscopy and Radiative Transfer, 186, 63–80, https://doi.org/10.1016/j.jqsrt.2016.06.026, 2017.

Snels, M., Scoccione, A., Liberto, L. D., Colao, F., Pitts, M., Poole, L., Deshler, T., Cairo, F., Cagnazzo, C., and Fierli, F.: Comparison of Antarctic polar stratospheric cloud observations by ground-based and space-borne lidar and relevance for chemistry–climate models, Atmospheric Chemistry and Physics, 19, 955–972, https://doi.org/10.5194/acp-19-955-2019, 2019.

Solomon, S.: Stratospheric ozone depletion: A review of concepts and history, Reviews of Geophysics, 37, 275–316, https://doi.org/10.1029/1999RG900008, 1999.

Spang, R., Hoffmann, L., Höpfner, M., Griessbach, S., Müller, R., Pitts, M. C., Orr, A. M. W., and Riese, M.: A multi-wavelength classification method for polar stratospheric cloud types using infrared limb spectra, Atmospheric Measurement Techniques, 9, 3619–3639, https://doi.org/10.5194/amt-9-3619-2016, 2016.

Spang, R., Hoffmann, L., Müller, R., Grooß, J.-U., Tritscher, I., Höpfner, M., Pitts, M., Orr, A., and Riese, M.: A climatology of polar stratospheric cloud composition between 2002 and 2012 based on MIPAS/Envisat observations, Atmospheric Chemistry and Physics, 18, 5089–5113, https://doi.org/10.5194/acp-18-5089-2018, 2018.

Toon, O. B., Hamill, P., Turco, R. P., and Pinto, J.: Condensation of HNO3 and HCl in the winter polar stratospheres, Geophysical Research Letters, 13, 1284–1287, https://doi.org/10.1029/GL013i012p01284, 1986.

Urban, J., Pommier, M., Murtagh, D. P., Santee, M. L., and Orsolini, Y. J.: Nitric acid in the stratosphere based on Odin observations from 2001 to 2009 – Part 1: A global climatology, Atmospheric Chemistry and Physics, 9, 7031–7044, https://doi.org/10.5194/acp-9-7031- 2009, 2009.

Voigt, C., Schreiner, J., Kohlmann, A., Zink, P., Mauersberger, K., Larsen, N., Deshler, T., Kro, C., Rosen, J., Adriani, A., Cairo, F., Donfrancesco, G. D., Viterbini, M., Ovarlez, J., Ovarlez, H., and David, C.: Nitric Acid Trihydrate (NAT) in Polar Stratospheric Clouds, Science, 290, 1756–1758, https://doi.org/10.1126/science.290.5497.1756, 2000.

Voigt, C., Schlager, H., Luo, B. P., Dörnbrack, A., Roiger, A., Stock, P., Curtius, J., Vössing, H., Borrmann, S., Davies, S., Konopka, P., Schiller, C., Shur, G., and Peter, T.: Nitric Acid Trihydrate (NAT) formation at low NAT supersaturation in Polar Stratospheric Clouds (PSCs), Atmospheric Chemistry and Physics, 5, 1371–1380, https://doi.org/10.5194/acp-5-1371-2005, 2005.

von König, M.: Using gas-phase nitric acid as an indicator of PSC composition, Journal of Geophysical Research, 107, https://doi.org/10.1029/2001jd001041, 2002.

Wang, D. Y., Blom, C. E., Ward, W. E., Fischer, H., Blumenstock, T., Hase, F., Keim, C., Liu, G. Y., Mikuteit, S., Oelhaf, H., Wetzel, G., Cortesi, U., Mencaraglia, F., Bianchini, G., Redaelli, G., Pirre, M., Catoire, V., Huret, N., Vigouroux, C., Mahieu, E., Demoulin, P.,Wood, S., Smale, D., Jones, N., Nakajima, H., Sugita, T., Urban, J., Murtagh, D., Boone, C. D., Bernath, P. F., Walker, K. a., Kuttippurath, J.,Toon, G., Piccolo, C., Brunswick, N., Zealand, N., Science, S., and Cedex, P.: Validation of MIPAS HNO3 operational data, Atmospheric Chemistry and Physics, 7, 4905–4934, https://doi.org/10.5194/acp-7-4905-2007, 2007.

Wang, X. and Michelangeli, D. V.: A review of polar stratospheric cloud formation, China Particuology, 4, 261–271, https://doi.org/10.1016/S1672-2515(07)60275-9, 2006.

Wegner, T., Grooß, J.-U., von Hobe, M., Stroh, F., Sumin´ska-Ebersoldt, O., Volk, C. M., Hösen, E., Mitev, V., Shur, G., and Müller, R.: Heterogeneous chlorine activation on stratospheric aerosols and clouds in the Arctic polar vortex, Atmospheric Chemistry and Physics, 12, 11 095–11 106, https://doi.org/10.5194/acp-12-11095-2012, 2012.

Wespes, C., Hurtmans, D., Clerbaux, C., and Coheur, P.-F.: O_3 variability in the troposphere as observed by IASI over 2008-2016: Contribution of atmospheric chemistry and dynamics, Journal of Geophysical Research: Atmospheres, 122, 2429–2451, https://doi.org/10.1002/2016JD025875, http://doi.wiley.com/10.1002/2016JD025875, 2017.

WMO: Scientific Assessment of Ozone Depletion: 2014, Global Ozone Research and Monitoring Project – Report No. 55, World Meteorological Organization, Geneva, Switzerland, 2014.

Zhu, Y., Toon, O. B., Lambert, A., Kinnison, D. E., Brakebusch, M., Bardeen, C. G., Mills, M. J., and English, J. M.: Development of a Polar Stratospheric Cloud Model within the Community Earth System Model using constraints on Type I PSCs from the 2010-2011 Arctic winter, Journal of Advances in Modeling Earth Systems, 7, 551–585, https://doi.org/10.1002/2015ms000427, 2015.